ICRP ref 4835-9252-8934
5 August 2015

Annals of the ICRP

ICRP PUBLICATION 1XX

The ICRP Computational Framework for Internal Dose Assessment for Reference Workers: Specific Absorbed Fractions

Editor
C.H. CLEMENT

Associate Editor
N. HAMADA

Authors on behalf of ICRP
W.E. Bolch, M. Zankl, K.F. Eckerman, T. Fell, A. Endo, J. Hunt,
D. Jokisch, K.P. Kim, and N. Petoussi-Henss

PUBLISHED FOR

The International Commission on Radiological Protection

by

[SAGE logo]

Please cite this issue as 'ICRP, 201Y. The ICRP Computational Framework for Internal Dose Assessment for Reference Workers: Specific Absorbed Fractions. ICRP Publication 1XX, Ann. ICRP 4X (0).'

34 **CONTENTS**
35

61

THE ICRP COMPUTATIONAL FRAMEWORK FOR INTERNAL DOSE ASSESSMENT FOR REFERENCE WORKERS: SPEFIFIC ABSORBED FRACTIONS

ICRP Publication 1XX

Approved by the Commission in Month Year

Abstract-Dose coefficients for assessment of internal exposures to radionuclides are radiological protection quantities giving either the organ equivalent dose or effective dose per intake of radionuclide following ingestion or inhalation. In the Commission's Occupational Intakes of Radionuclides (OIR) series of documents, new biokinetic models for distribution of internalised radionuclides in the human body are presented as needed for establishing time-integrated activity within organs of deposition (source organs). These series of reports replace *Publications 30* and *68*. In addition, other fundamental data needed for computation of the dose coefficients are radionuclide decay data (energies and yields of emitted radiations), which are given in *Publication 107*, and values of specific absorbed fraction (SAF) – defined as the fraction of the particle energy emitted in a source tissue region that is deposited in a target tissue region per mass of target tissue (units of kg^{-1}). This report provides the technical basis for SAFs relevant to internalised radionuclide activity in the organs of the reference adult male and reference adult female as defined in *Publications 89* and *110*. SAFs are given for uniform distributions of monoenergetic photons, electrons, alpha particles, and fission-spectrum neutrons over a range of relevant energies. Electron SAFs include both their collision and radiative components of energy deposition. SAF data are matched to source and target organs of the biokinetic models of the OIR publication series, as well as the *Publication 100* alimentary tract model and the *Publication 66* respiratory tract model, the latter as revised within *Publication 130* – OIR Part 1. The document further outlines the computational methodology and nomenclature for assessment of internal dose in a manner consistent with that used for nuclear medicine applications. Numerical data for particle specific and energy dependent SAFs are given in electronic format for numerical coupling to the respiratory tract, alimentary tract, and systemic biokinetic models of the OIR publication series.

Keywords: Computational phantom, Absorbed fraction, Specific absorbed fraction, Radiation transport, Internal dosimetry

AUTHORS ON BEHALF OF ICRP

W.E. Bolch, M. Zankl, K.F. Eckerman, T. Fell, A. Endo, J. Hunt,
D. Jokisch, K.P. Kim, and N. Petoussi-Henss

PREFACE

The membership of the Task Group on Dose Calculations (DOCAL) at the time of the completion of this report was:

Members:

W.E. Bolch (Chair)	T.P. Fell	D. Nosske
V. Berkovski	N.E. Hertel	N. Petoussi-Henss
L. Bertelli	J.G.S. Hunt	M. Pelliccioni
A. Endo	N. Ishigure	M. Zankl
K.F. Eckerman		

Corresponding Members:

A. Birchall	C. Lee	R. Tanner
G. Gualdrini	H. Schlattl	X.G. Xu
D. Jokisch	M. Stabin	

The membership of the Task Group on Internal Dosimetry (INDOS) at the time of the completion of this report was:

Members:

F. Paquet (Chair)	H. Doerfel	J.D. Harrison
E. Ansoborlo	G. Etherington	R.W. Leggett
M.R. Bailey	A. Giussani	J. Lipsztein
E.J.A. Blanchardon	R.A. Guilmette	D. Melo

Corresponding Members:

A. Bouville	C. Hurtgen	D. Nosske
C-M. Castellani	A. Luciani	D.M. Taylor
R. Cruz-Suarez	D. Newton	D. Whillans

The membership of Committee 2 during the period of preparation of this report was:

(2009-2013)

H-G. Menzel (Chair)	R. Cox	R. Leggett
M.R. Bailey	G. Dietze	J.L. Lipsztein
M. Balonov	K.F. Eckerman	J. Ma
D. Bartlett	A. Endo	F. Paquet
V. Berkovski	J.D. Harrison	N. Petoussi-Henss
W.E. Bolch	N. Ishigure	A.S. Pradhan

(2013-2017)

J.D. Harrison (Chair)	M. Degteva	D. Noβke
M.R. Bailey	A. Endo	F. Paquet
V. Berkovski	J.G. Hunt	N. Petoussi-Henss

151	L. Bertelli	C. Hyeong Kim	F. Wissmann
152	W.E. Bolch	R. Leggett	
153	D. Chambers	J. Ma	
154			

MAIN POINTS

- **Dose coefficients for assessment of internal exposure to radionuclides following inhalation and ingestion require the use of biokinetic models (*Publication 130*), radionuclide decay scheme data (*Publication 107*), and values of specific absorbed fraction in a computational phantom.**
- **Specific absorbed fractions are defined as the fraction of particle energy emitted in a source tissue region that is deposited in a target tissue region per mass of target tissue, and are expressed in units of kg^{-1}.**
- **This report presents reference values of the specific absorbed fraction (SAF) for internally emitted photons, electrons, and alpha particles, as well as fission-spectrum neutrons associated with radionuclides that decay by spontaneous fission.**
- **The majority of SAF values given in this report are derived from Monte Carlo radiation transport simulations in the ICRP Reference Adult Male and Reference Adult Female computational phantoms defined in *Publication 110*.**
- **Additional values of electron and alpha particle SAFs are taken from *Publication 66* for the Human Respiratory Tract Model, with changes consistent with revisions to the HRTM presented in *Publication 130*.**
- **In this report, new values of electron and alpha particle SAFs are given for the Human Alimentary Tract Model that supercede those given in *Publication 100*.**
- **The reference SAFs presented in this report are numerically coupled to the compartmental models of the HRTM, HATM, and the systemic biokinetic models of *Publication 130* in the calculation of reference dose coefficients for both organ equivalent dose and effective dose.**

GLOSSARY

Absorbed dose, D

The absorbed dose is given by

$$D = \frac{\mathrm{d}\bar{\varepsilon}}{\mathrm{d}m}$$

where $\mathrm{d}\bar{\varepsilon}$ is the mean energy imparted by ionising radiation to matter of mass $\mathrm{d}m$. The SI unit of absorbed dose is joule per kilogramme (J kg^{-1}), and its special name is gray (Gy).

Absorbed fraction (AF), $\phi(r_T \leftarrow r_S, E_{R,i})$

Fraction of energy $E_{R,i}$ of the i^{th} radiation of type R emitted within the source region r_S that is absorbed in the target region r_T. These target regions may be tissues (e.g. liver) or they may be cell layers within organs (e.g. stem cells of the stomach wall) (see definitions for 'Target Region' and 'Target Tissue').

Active (bone) marrow

Active marrow is haematopoietically active and gets its red colour from the large numbers of erythrocytes (red blood cells) being produced. Active bone marrow serves as a target region for radiogenic risk of leukaemia.

Activity

The number of nuclear transformations of a radioactive material during an infinitesimal time interval, divided by its duration(s). The SI unit of activity is the becquerel (Bq): 1 Bq = 1 s^{-1}

Becquerel (Bq)

Special name for the SI unit of activity. 1 Bq = 1 s^{-1}, 1 MBq =10^6 Bq.

Biological half-life

The time required for a compartment of a biological system to eliminate (in the absence of additional input and radioactive decay) half of its radionuclide content.

Bone marrow [see also 'Active (bone) marrow'; 'Inactive (bone) marrow']

Bone marrow is a soft, highly cellular tissue that occupies the cylindrical cavities of long bones and the cavities defined by the bone trabeculae of the axial and appendicular skeleton. Total bone marrow consists of a sponge-like, reticular, connective tissue framework called stroma, myeloid (blood-cell-forming) tissue, fat cells (adipocytes), small accumulations of lymphatic tissue, and numerous blood vessels and sinusoids. There are two types of bone marrow: active (red) and inactive (yellow) where these adjectives refer to the marrow's potential for blood cell element production (haematopoiesis).

Committed effective dose, $E(\tau)$. See also 'Effective Dose'.

In the Occupational Intakes of Radionuclides (OIR) report series, the integration time τ following the intake is taken to be 50 years. The committed effective dose $E(50)$ is calculated with the use of male and female committed equivalent doses to individual target organs or tissues, T according to the expression:

$$E(50) = \sum_T w_T \cdot \left[\frac{H_T^M(50) + H_T^F(50)}{2} \right]$$

The SI unit for committed effective dose is the same as for absorbed dose, J kg^{-1}, and its special name is sievert (Sv).

Committed equivalent dose $H_T(50)$. See also 'Equivalent Dose'.

In the OIR report series, the equivalent dose to an organ or tissue region is calculated using a 50-year commitment period. It is taken as the time integral of the equivalent dose rate in a target organ or tissue T of the Reference Adult Male or the Reference Adult Female. These in turn are predicted by reference biokinetic and dosimetric models following the intake of radioactive material into the body of the Reference Worker. The integration period is thus 50 years following the intake:

$$H_T(50) = \int_0^{50} \dot{H}(r_T, t)\, dt$$

For both sexes, the equivalent dose rate $\dot{H}(r_T, t)$ in target region r_T at time t after an acute intake is expressed as:

$$\dot{H}(r_T, t) = \sum_{r_S} A(r_S, t) \cdot S_w(r_T \leftarrow r_S)$$

where:

$A(r_S, t)$ is the activity of the radionuclide in source region r_S at time t after intake, in Bq, as predicted by the reference biokinetic models for Reference Worker,

$S_w(r_S \leftarrow r_T)$ is the radiation-weighted S coefficient; i.e. the equivalent dose to target region r_T per nuclear transformation in source region r_S, in Sv $(Bq\ s)^{-1}$, for the Reference Adult Male and Female.

The SI unit for committed equivalent dose is the same as for absorbed dose, J kg^{-1}, and its special name is sievert (Sv).

Dose coefficient

For adult workers, a dose coefficient is defined as either the committed equivalent dose in organ or tissue T per intake, $H_T(50)$, or the committed effective dose per intake, $E(50)$, where 50 is the dose-commitment period in years over which the dose is calculated. Note that elsewhere the term 'dose per intake coefficient' is sometimes used for dose coefficient.

Effective dose, E

In accordance with the generic definition of effective dose in *Publication 103*, the effective dose is calculated as:

$$E = \sum_T w_T \left[\frac{H_T^M + H_T^F}{2} \right]$$

where H_T^M and H_T^F are the equivalent doses to the tissues or organs r_T of the Reference Adult Male and Female, respectively, and w_T is the tissue weighting factor for target tissue T, with $\sum_T w_T = 1$. The sum is performed over all organs and tissues of the human body considered to be sensitive to the induction of stochastic effects. Since w_R and w_T are dimensionless, the SI unit for effective dose is the same as for absorbed dose, J kg^{-1}, and its special name is sievert (Sv).

Endosteum (or endosteal layer)

A 50-µm-thick layer covering the surfaces of the bone trabeculae in regions of trabecular spongiosa and those of the cortical surfaces of the medullary cavities within the shafts of all long bones. It is assumed to be the target region for radiogenic bone cancer. This target region replaces that previously introduced in *Publications 26* and *30* – the bone surfaces – which had been defined as a single cell layer, 10 µm in thickness, covering the surfaces of both the bone trabeculae and the Haversian canals of cortical bone.

Equivalent dose (H_T)

The equivalent dose to a tissue or organ is defined as:

$$H_T = \sum_R w_R D_{R,T}$$

where w_R is the radiation weighting factor for radiation type R, and $D_{R,T}$ is the organ absorbed dose from radiation type R in a tissue or organ r_T of the Reference Adult Male or Female. Since w_R is dimensionless, the SI unit for the equivalent dose is the same as for absorbed dose, J kg^{-1}, and its special name is sievert (Sv).

Gray (Gy)

The special name for the SI unit of absorbed dose: 1 Gy = 1 J kg^{-1}.

Inactive (bone) marrow

In contrast to the active marrow, the inactive marrow is haematopoietically inactive (i.e. does not directly support haematopoiesis). It gets its yellow colour from fat cells (adipocytes) that occupy most of the space of the bone marrow framework.

Marrow cellularity

The fraction of bone marrow volume in a given bone that is haematopoietically active. Age- and bone-site-dependent reference values for marrow cellularity are given in Table 41 of *Publication 70*. As a first approximation, marrow cellularity may be thought of as 1 minus the fat fraction of bone marrow.

Mean absorbed dose, $D_{R,T}$

The mean absorbed dose in a specified organ or tissue region r_T is given by

$D_T = 1/m_T \int D \, dm$, where m_T is the mass of the organ or tissue, and D is the absorbed dose in the mass element dm. The SI unit of mean absorbed dose is joule per kilogramme (J kg^{-1}), and its special name is gray (Gy).

Other tissues

A term used in biokinetic models to represent all other tissues that are not already identified explicitly in the biokinetic model structure.

Other soft tissues

A term used in biokinetic models to represent all other tissues that are not already identified explicitly in the biokinetic model structure, with the exclusion of mineral bone in its cortical and trabecular forms.

Radiation weighting factor, w_R

A dimensionless factor by which the organ or tissue absorbed dose component of a radiation type R is multiplied to reflect the relative biological effectiveness of that radiation type. It is used to derive the organ equivalent dose from the mean absorbed dose in an organ or tissue.

Red (bone) marrow

See ‘Active (bone) marrow’.

Reference Male and Reference Female

An idealised male or female with anatomical and physiological characteristics defined by ICRP for the purpose of radiological protection.

Reference parameter value

The value of a parameter, factor or quantity that is regarded as valid for use in dosimetric calculations and recommended by ICRP. These values are fixed and are not subject to uncertainties.

Reference Person

An idealised person, for whom the equivalent doses to organs and tissues are calculated by averaging the corresponding doses of the Reference Male and Female. The equivalent doses of the Reference Person are used for the calculation of the effective dose.

Reference phantom

The computational phantom of the human body (male or female voxel phantom based on medical imaging data), defined in *Publication 110* with the anatomical and physiological characteristics of the Reference Male and Female defined in *Publication 89*.

Reference Worker

An adult Reference Person combined with the reference biokinetic and dosimetric models and their parameter values, as defined in this report series for the Reference Worker (systemic biokinetic models, the Human Respiratory Tract Model, the Human Alimentary Tract Model, and dosimetric models). The structure and parameter values of biokinetic models of the Reference Worker are invariant on the sex, age, race and other individual-specific characteristics, but based on reference male parameter values where sex-specific models are available.

Sievert (Sv)

The special name for the SI unit (J kg^{-1}) of equivalent dose and effective dose.

Source region (r_s)

Region of the body containing the radionuclide. The region may be an organ, a tissue, the contents of the alimentary tract or urinary bladder, or the surfaces of tissues as in the skeleton and the respiratory tract.

Specific absorbed fraction (SAF), $\Phi(r_T \leftarrow r_S, E_{R,i})$

Fraction of radiation R of energy $E_{R,i}$ emitted within the source region r_S that is absorbed per mass in the target region r_T.

Spongiosa

Term referring to the combined tissues of the bone trabeculae and marrow tissues (both active and inactive) located beneath cortical bone cortices across regions of the axial and appendicular skeleton. Spongiosa is one of three bone regions defined in the *Publication 110* reference phantoms, the other two being cortical bone and medullary marrow of the long bone shafts. As the relative proportions of trabecular bone, active marrow, and inactive marrow vary with skeletal site, the homogeneous elemental composition and mass

density of spongiosa are not constant but vary with skeletal site (see Annex B of *Publication 110*).

S-coefficient (radiation-weighted) $S_w(r_T \leftarrow r_S)$

The equivalent dose to target region r_T per nuclear transformation of a given radionuclide in source region r_S, Sv (Bq s)$^{-1}$, for the Reference Adult Male and Reference Adult Female.

$$S_w(r_T \leftarrow r_S) = \sum_R w_R \sum_i E_{R,i}\, Y_{R,i}\ \Phi\left(r_T \leftarrow r_S, E_{R,i}\right)$$

where

$E_{R,i}$ is the energy, in joules, of the i^{th} radiation of type R emitted in nuclear transformations of the radionuclide;

$Y_{R,i}$ is the yield of the i^{th} radiation of type R per nuclear transformation, (Bq s)$^{-1}$,

w_R is the radiation weighting factor for radiation type R (Table 1),

$\Phi\left(r_T \leftarrow r_S, E_{R,i}\right)$ is the specific absorbed fraction (SAF), defined as the fraction of energy $E_{R,i}$ of radiation type R emitted within the source region r_S that is absorbed per mass in the target region r_T, kg^{-1}.

Note that no change in anatomical parameters with time (age) are considered for adults; in this case, therefore, S_w is invariant with respect to time and its value represents either the equivalent dose rate (Sv s^{-1}) per activity (Bq), or the equivalent dose (Sv) per nuclear transformation (Bq-s) in the target region.

Target region (r_T)

Organ or tissue region of the body in which a radiation absorbed dose is received.

Target tissue (T)

Organ or tissues in the body for which tissue weighting factors are assigned in the effective dose (Table 2). In many cases, each target tissue T corresponds to a single target region r_T. In the case of extrathoracic region, thoracic region, colon, and lymphatic nodes, however, a fractional weighting of more than one target region r_T defines the target tissue T (Table 3).

Tissue weighting factor, w_T. See also 'Effective Dose'.

The factor by which the equivalent dose to an organ or tissue r_T is weighted to represent the relative contribution of that organ or tissue to overall radiation detriment from stochastic effects. It is defined as

391 $$\sum_{T} w_T = 1$$

392

1. INTRODUCTION

(1) The system of radiological protection recommended by the International Commission on Radiological Protection (ICRP) is the basis for standards and working practices throughout the world (ICRP, 1991, 2007; IAEA, 1996). Fundamental to the application of ICRP recommendations are the protection quantities defined by ICRP, equivalent dose and effective dose. While the definition of these quantities remains unchanged in the most recent recommendations (ICRP, 2007), there have been important changes that affect the values calculated per radiation exposure. Committee 2 of ICRP is responsible for the provision of these reference dose coefficients for the assessment of internal radiation exposure, calculated using reference biokinetic and dosimetric models, and reference data for workers and members of the public. Following the 2007 Recommendations (ICRP, 2007), Committee 2 and its Task Groups engaged in a substantial programme of work to provide new dose coefficients for various circumstances of radiation exposure.

(2) The underlying foundations of radionuclide dose coefficients for internal exposures include several reference parameters and models. These include, among others, (i) masses of organs and tissues in the Reference Adult Male and Female, (ii) radionuclide decay information, (iii) biokinetic models for inhalation, ingestion, and systemic biodistribution, and (iv) values of specific absorbed fractions (SAFs). *Publications 89* and *107* (ICRP, 2002a, 2008) provide reference organ masses and radionuclide decay data, respectively, as needed for calculations of internal dose coefficients. *Publications 66* and *100* (ICRP, 1994a, 2006) provide models for inhalation and ingestion of radionuclides, respectively. Presently, the ICRP Task Group on Internal Dose Coefficients (IDC) is completing an extensive set of revisions to its systemic biokinetic models within its Occupational Intakes of Radionuclides (OIR) series of documents. The purpose of this report, prepared by the ICRP Task Group on Computational Phantoms and Radiation Transport (CPRT), is to document the development and provide data for SAFs for a wide range of internally emitted radiations – photons, electrons, alpha particles, and in the case of radionuclides undergoing spontaneous fission, neutrons – for all relevant combinations of source and target tissues. The SAF is defined as the fraction of radiation energy emitted within a source region that is absorbed per mass in a target region. These tissue regions can be whole organs, organ sub-regions, individual cell layers, or tissue interface surfaces. The values given in this report are for the ICRP Reference Adult Male and Reference Adult Female, as defined in *Publication 103* (ICRP, 2007), and are used within the OIR report series in the calculation of ICRP reference dose coefficients for inhalation and ingestion. Further information is given in the OIR Part 1 (ICRP, 2015).

2. ICRP SCHEMA FOR INTERNAL DOSE ASSESSMENT

(3) The ICRP dosimetry schema is presented below as applied to assessment of organ equivalent dose and effective dose following intakes of radionuclides. The system involves numerical solution of reference biokinetic models, yielding the time-dependent number of nuclear transformations in various source tissues. These solutions are then coupled with reference data on nuclear decay information, target tissue masses, and fractions of emitted energy released from source tissue regions that are deposited in target tissue regions as defined in the *Publication 110* Reference Phantoms (ICRP, 2009). Presented below is the computational formalism of these dosimetry calculations consistent with the protection quantities defined in *Publication 103* (ICRP, 2007).

(4) As defined in *Publication 103* (and this document's Glossary), the effective dose employs two forms of weighting factors. The first is the radiation weighting factor w_R used in the calculation of the organ equivalent dose (in Sv) given computed values of organ absorbed dose (in Gy). Values of w_R are shown in Table 1. The second is the tissue weighting factor w_T used in the calculation of the effective dose (in Sv) given computed values of sex-averaged organ equivalent doses. Values of w_T are shown in Table 2.

Table 1. ICRP radiation weighting factors

Radiation Type	Radiation Weighting Factor, w_R
Photons	1
Electrons and muons	1
Protons and charged pions	2
Alpha particles, fission fragments, heavy ions	20
Neutrons	Continuous function of neutron energy See Eqn. 4.3 of *Publication 103*

Table 2. ICRP tissue weighting factors.

Tissue	w_T	$\sum w_T$
Bone-marrow, breast, colon, lung, stomach, remainder tissues *(13*)*	0.12	0.72
Gonads	0.08	0.08
Urinary bladder, oesophagus, liver, thyroid	0.04	0.16
Bone surface, brain, salivary glands, skin	0.01	0.04

*Remainder Tissues: adrenals, extrathoracic (ET) regions of the respiratory tract, gall bladder, heart, kidneys, lymphatic nodes, muscle, oral mucosa, pancreas, prostate (male), small intestine, spleen, thymus, uterus/cervix (female).

2.1.Computational solutions to the ICRP reference biokinetic models

(5) The Human Respiratory Tract Model (HRTM) (ICRP, 1994a), the Human Alimentary Tract Model (HATM) (ICRP, 2006), and the systemic biokinetic models of this report describe the dynamic behaviour of radionuclides within the body. Given the routes of intake, the models predict the subsequent uptake to the systemic circulation, the distribution among tissues of the body, and the routes of elimination from the body. Superimposed on these dynamics are in situ radioactive decay and the ingrowth of radioactive progeny. Consequently, the uptake, distribution, and elimination of all decay products are predicted, in addition to those of the parent radionuclide.

(6) The compartment models of the respiratory and alimentary tract coupled with those of the systemic biokinetics define a system of first-order differential equations. The solution to the set of equations is the time-dependent distribution of the radionuclide and its radioactive progeny, if any, in mathematical compartments (pools) that are associated with anatomical regions in the body. Let $A_{i,j}(t)$ represent the activity of radionuclide i in compartment j at time t. The rate of change in the activity of member i of the decay chain, i =1, 2, …, N with i = 1 being the parent nuclide, in compartment j, can be written as:

$$\frac{dA_{i,j}(t)}{dt} = \sum_{\substack{k=1 \\ k\neq j}}^{M} A_{i,k}\,\lambda_{i,k,j} - A_{i,j}\left[\sum_{\substack{k=1 \\ k\neq j}}^{M} \lambda_{i,j,k} + \lambda_i^P\right] + \sum_{k=1}^{i-1} A_{k,j}\,\beta_{k,i}\,\lambda_i^P \qquad (2.1)$$

where :

M is the number of compartments describing the kinetics;

$\lambda_{i,j,k}$ is the fractional transfer rate of chain member i from compartment j (donor compartment) to compartment k (receiving compartment) in the biokinetic model;

λ_i^P is the physical decay constant of chain member i; and

$\beta_{k,i}$ is the fraction of the decays of chain member k forming member i.

(7) Given the initial conditions specified for the compartments, $A_{i,j}(0)$, Eqn. 2.1 defines the dynamic behaviour of the radionuclide and its progeny within the human body. The first term on the right-hand side of Eqn. 2.1 represents the rate of flow of chain member i into compartment j from all donor compartments. The second term represents the rate of removal of member i from compartment j both by transfer to receiving compartments and by physical decay. The third term addresses the ingrowth of member i within compartment j due to the presence of its precursors k in the compartment. Note that the members of the decay chain are assumed to be of order such that the precursors of member i have indices less than i. An ordered listing of the chain members can be obtained using the DECDATA software distributed with *Publication 107* (ICRP, 2008).

(8) The system of N x M ordinary first-order differential equations must be solved using suitable numerical methods. The system is generally solved for the initial conditions that $A_{i,j}(0) = 0$ for all compartments with the exception of compartments of intake where nonzero initial conditions are only applied to the parent nuclide; i.e. $i = 1$. In the case of inhalation of radon and its progeny, nonzero initial conditions may be assigned to progeny within the compartments of the respiratory tract (i.e. inhalation of short-lived radon progeny in the inspired air).

(9) To calculate the numerical values of the dose coefficients, it is necessary to associate the biokinetic compartments of Eqn 2.1 with anatomical regions in the body; so-called source regions indexed by r_S. The source regions may or may not be a living tissue; e.g. the contents of the alimentary tract is not a living tissue, and may consist of more than one kinetic compartment. The number of nuclear transformations of chain member *i* occurring in source region r_S, $\tilde{A}_i(r_S)$ (Bq s), is given by:

$$\tilde{A}_i(r_S, \tau) = \sum_j \int_0^\tau A_{i,j}(t)\, dt \tag{2.2}$$

where τ is the commitment period (taken to be 50 y for workers). The summation in Eqn 2.2 is over all kinetic compartments *j* associated with source region r_S and the quantity $A_{i,j}(t)$ is obtained by solving Eqn 2.1. The number of nuclear transformations per activity intake in the source region r_S, denoted as $\tilde{a}_i(r_S, \tau)$ (s), is given by:

$$\tilde{a}_i(r_S, \tau) = \frac{\tilde{A}_i(r_S, \tau)}{\sum_j A_{1,j}(0)} \tag{2.3}$$

where the summation in the denominator is over the compartment contents at $t = 0$. In the case of inhalation of particulate and gaseous matter, the denominator includes the exhaled activity as only a fraction of the activity intake that is deposited in the compartments of the HRTM.

2.2. Computation of ICRP reference dose coefficients for equivalent dose

(10) The committed equivalent dose coefficient in target region r_T of the Reference Adult Male, $h^M(r_T, \tau)$, and Reference Adult Female, $h^F(r_T, \tau)$, for integration time t is given by

$$h^M(r_T, \tau) = \sum_i \sum_{r_S} \tilde{a}_i(r_S, \tau)\; S_w^M\,(r_T \leftarrow r_S)_i \tag{2.4}$$

$$h^F(r_T,\tau) = \sum_i \sum_{r_S} \tilde{a}_i(r_S,\tau)\ S_w^F\,(r_T \leftarrow r_S)_i \qquad (2.5)$$

where the S coefficients, $S_w^M(r_T \leftarrow r_S)_i$ and $S_w^F(r_T \leftarrow r_S)_i$, are the radiation-weighted equivalent doses in target region r_T per nuclear transformation of chain member i in source region r_S [Sv (Bq s)$^{-1}$] for the male and female worker, respectively. Note that the outer summation extends over the parent nuclide and its progeny.

(11) A number of tissues listed in Table 2 used to compute the effective dose are considered to be represented by a single target region r_T. In cases where more than one tissue region defines the target tissue, fractional weighting of the equivalent dose must be made. The committed equivalent dose coefficients for tissue T in the Reference Adult Male, $h_T^M(\tau)$, and Reference Adult Female, $h_T^F(\tau)$, are thus given as:

$$h_T^M(\tau) = \sum_{r_T} f(r_T,T)\ h^M(r_T,\tau) \qquad (2.6)$$

$$h_T^F(\tau) = \sum_{r_T} f(r_T,T)\ h^F(r_T,\tau) \qquad (2.7)$$

where the target region fractional weights $f(r_T,T)$ are the proportions of the equivalent dose in tissue T associated with target region r_T. With the exception of the tissues addressed in Table 3, the tissues of Table 2 are represented by a single target region and thus for these tissues $f(r_T,T) = 1$. In Table 3, the values $f(r_T,T)$ for the ET and thoracic (TH or lung) regions are taken to be equivalent to their risk apportionment factors as assigned in the revised HRTM. For the colon, values of $f(r_T,T)$ are taken to be the fractional masses of the stem cell layers within the alimentary tract walls in *Publication 100* (ICRP, 2006). For the lymphatic nodes, values of $f(r_T,T)$ are taken to be the fractional masses of lymphatic nodes (not lymphatic tissues) within the extrathoracic, thoracic, and non-respiratory regions consistent with data given in *Publication 66* (ICRP, 1994).

Table 3. Target region fractional weights, $f(r_T,T)$

Tissue, T	r_T	$f(r_T,T)$
ET region	ET_1 (anterior nose)	0.001
	ET_2 (posterior nasal passages larynx and pharynx)	0.999
Lung (Thoracic)	BB (bronchial)*	1/3
	bb (bronchiolar)	1/3
	AI (alveolar-interstitial)	1/3
Colon	Right colon	0.4
	Left colon	0.4
	Rectosigmoid	0.2
Lymphatic nodes	LN_{ET}	0.08
	LN_{TH}	0.08

Lymph (systemic)	0.84

* The basal and secretory cells are the two target regions weighted equally.

2.3. Computation of ICRP reference dose coefficients for effective dose

(12) As defined in *Publication 103* (ICRP, 2007), the committed effective dose coefficient, $e(\tau)$, is then:

$$e(\tau) = \sum_T w_T \left[\frac{h_T^M(\tau) + h_T^F(\tau)}{2}\right] \tag{2.8}$$

where w_T is the tissue weighting factor for target tissue T and $h_T^M(\tau)$ and $h_T^F(\tau)$ are the corresponding committed equivalent dose coefficients for these same tissues in the Reference Adult Male and Reference Adult Female, respectively.

2.4. Implementation of specific absorbed fractions within the ICRP system

(13) The radiation-weighted S coefficient [Sv (Bq-s)$^{-1}$] for a radionuclide is calculated as:

$$S_w(r_T \leftarrow r_S) = \sum_R w_R \sum_i E_{R,i}\, Y_{R,i}\ \Phi\left(r_T \leftarrow r_S, E_{R,i}\right) \tag{2.9}$$

where

$E_{R,i}$ is the energy of the i^{th} radiation of type R emitted in nuclear transformations of the radionuclide;

$Y_{R,i}$ is the yield of the i^{th} radiation of type R per nuclear transformation, [(Bq s)$^{-1}$];

w_R is the radiation weighting factor for radiation type R (Table 1); and

$\Phi\left(r_T \leftarrow r_S, E_{R,i}\right)$ is the SAF, defined as the fraction of energy $E_{R,i}$ of radiation type R emitted within the source tissue r_S that is absorbed per mass in the target tissue r_T (kg^{-1}).

(14) The energies and yields of the emitted radiations, $E_{R,i}$ and $Y_{R,i}$, are taken from *Publication 107* (ICRP, 2008). For β emissions, the spectral data are used in the calculation of S_w rather than mean values; i.e. the inner summation in Eqn. 9 is replaced by the integral over the spectrum.

(15) SAF values given in this report are calculated as the ratio of the absorbed fraction (AF) and the target organ mass. Values of reference organ masses used in SAF calculations are listed in Annex A of this report and are assumed to be inclusive of the organ blood content. Values of the absorbed fraction are calculated by radiation

transport simulation using either voxelised or stylised (mathematically defined) geometries as outlined further in Chapters 3 to 6.

2.5. Derivation of specific absorbed fractions for distributed source organs

(16) Systemic biokinetic models indicate radionuclide deposition from blood to various identified source regions r_S, each with its own compartmental representation in the biokinetic model. In many instances, the balance of radionuclide deposition from blood will be assigned to "other tissues" of the body, which implies all other soft tissues not previously identified as source organs. To address this source region, which is generally unique to a given radionuclide biokinetic model, one must derive the SAF for the relevant target tissues r_T. This SAF may be calculated using the so-called additive approach as:

$$SAF(r_T \leftarrow Other) = \frac{1}{M_{Other}} \sum_{r_S} M_{r_S} \, SAF(r_T \leftarrow r_S) \tag{2.10}$$

where the summation is over source regions not explicitly included in the systemic biokinetic model. Unless specifically noted in the biokinetic model, deposition to other tissues is not assigned to mineral bone in either its cortical or trabecular form. A summary of reference source tissue masses is given in Table A.2.

3. COMPUTATIONAL METHODS FOR WHOLE BODY ORGANS

3.1. The ICRP / ICRU reference computational phantoms

(17) For the computations of organ absorbed doses, the adult male and female reference computational phantoms, representing the ICRP Reference Adult Male and Reference Adult Female (ICRP, 2007) were used in this report. These phantoms were adopted by the ICRP and ICRU as the phantoms for the computation of the ICRP reference dose coefficients and are extensively described in *Publication 110* (ICRP, 2009). The reference computational phantoms are digital three-dimensional (3D) representations of human anatomy and are based on human computed tomographic (CT) data. They are consistent with the information given in *Publication 89* (ICRP, 2002) on the reference anatomical parameters for both male and female adults. The reference computational phantoms (or models) were constructed by modifying the voxel models (Zankl and Wittmann, 2001; Zankl et al., 2005) of two individuals (Golem and Laura) whose body height and mass closely resembled the reference data. The organ masses of both phantoms were adjusted to the ICRP data on the Reference Male and Reference Female with high precision, without significantly altering their realistic anatomy. The phantoms contain all target regions relevant to the assessment of human exposure to ionising radiation for radiological protection purposes, i.e. all organs and tissues that contribute to the quantity effective dose (ICRP, 2007).

(18) Each phantom is represented in the form of a 3D array of cuboid voxels. Each voxel is a volume element, and the voxels are arranged in columns, in rows, and in slices. Each entry in the array identifies the organ or tissue to which the corresponding voxel belongs. The male reference computational phantom consists of approximately 1.95 million tissue voxels (excluding voxels representing the surrounding vacuum) each with a slice thickness (corresponding to the voxel height) of 8.0 mm and an in-plane resolution (i.e. voxel width and depth) of 2.137 mm, corresponding to a voxel volume of 36.54 mm^3. The number of slices is 220, resulting in a body height of 1.76 m; the body mass is 73 kg. The female reference computational phantom consists of approximately 3.89 million tissue voxels, each with a slice thickness of 4.84 mm and an in-plane resolution of 1.775 mm, corresponding to a voxel volume of 15.25 mm^3. The number of slices is 346, and the body height is 1.63 m; the body mass is 60 kg. The number of individually segmented structures is 136 in each phantom, and 53 different tissue compositions have been assigned to them. The various tissue compositions reflect both the elemental composition of the tissue parenchyma (ICRU, 1992a) and each organ's blood content (ICRP, 2002) (i.e. organ composition inclusive of blood). Fig. 1 shows frontal (coronal) views of the male (left) and female (right) computational phantom, respectively.

(19) Due to the limited resolution of the tomographic data on which these phantoms are based and the very small dimensions of some of the source and target regions, not all tissues could be explicitly represented. In the skeleton, for example, the target tissues of interest are the red bone marrow in the marrow cavities of spongiosa and the endosteal layer lining these cavities (presently assumed to be 50 μm in thickness). Due to their small dimensions, these two target tissues had to be

incorporated as homogeneous constituents of spongiosa within the reference phantoms. At lower energies of photon and neutrons, secondary charged-particle equilibrium is not fully established in these tissue regions over certain energy ranges. More refined techniques for accounting for these effects in skeletal dosimetry are discussed in Chapter 4.

Fig. 1. Images of the adult male (left) and adult female (right) computational phantoms. The following organs can be identified by different surface colours: breast, bones, colon, eyes, lungs, liver, pancreas, small intestine, stomach, teeth, thyroid and urinary bladder. Muscle and adipose tissue are semi-transparent. For illustration purposes, the voxelised surfaces have been smoothed.

(20) Similarly, the fine structure of some of the target regions in the human respiratory tract (HRT) and human alimentary tract (HAT) could not be described by the voxel geometry of the reference phantoms, and thus stylised models of the airways and of individual segments of the alimentary tract were employed for electrons and alpha particles in the respiratory and alimentary tracts. However, for photon SAFs and for electron cross-irradiation SAFs from and to source and target regions outside the HRT and HAT, the representations of these two organ systems as described in the reference computational phantoms were used.

(21) Small differences exist in the masses of the target tissues in the computational phantom (given in Annex D of *Publication 110*) and the masses given in Table A.1 of this report, as the latter includes the blood content of the target tissue. For cross-fire geometries, Petoussi-Henss et al. (2007) demonstrate the principle given in MIRD Pamphlet No. 5, Revised (Snyder et al., 1978) and MIRD Pamphlet No. 11 (Snyder et al. 1975) that the SAF is independent of target mass. Consequently, all cross-fire SAFs were calculated with the computational phantoms (Zankl et al., 2012), according to the specifications of the source and target regions as given in Annex C (soure regions) and Annex D (target regions) of *Publication 110.* A summary of source tissue masses is correspondingly given in Table A.2.

(22) Self-irradiation SAFs for all radiation types were calculated by taking the self-irradiation AFs from the computational phantoms and dividing by the target mass given in Table A.1 of this report. For self-irraidation geometries, Snyder (1970) described the photon absorbed fraction varying in proportion to the cube root of the target mass. This proportionality holds for photon energies and media where Compton scattering is the dominant interaction. Since the differences in the computational phantom organ mass and the reference target mass are small, simply dividing the derived AF by the reference target mass results in only small absolute differences in the SAF while allowing for an improved SAF at low photon energies.

(23) The blood source is an exception to the above cross-fire discussion, as the blood content of the target contributed significantly to the energy deposition in the target tissue. Thus, the target tissue SAF for the blood source for all radiations were calculated by taking the cross-fire irradiation AFs and dividing by the target mass given in Table A.1 of this report.

(24) This discussion does not apply to epithelial targets for the HATM and HRTM as they are specificied in terms of a tissue layer at depth.

3.2. Radiation transport codes used for absorbed fraction calculations

3.2.1. Photon and electron transport calculations

(25) For calculations of photon and electron absorbed fractions used in this report for reporting corresponding SAFs, the electron-gamma-shower code system EGSnrc Version v4-2-3-0 has been used (Kawrakow et al., 2009). This code is an extended and improved version of EGS4 (Nelson et al., 1985), maintained by the National Research Council of Canada (NRC). The transport of photons and electrons can be simulated for particle kinetic energies from a few keV up to several hundred GeV, although simulations performed in this study were made over the energy range of 10 keV to 10 MeV. Values below 10 keV were determined via extrapolation.

(26) For photon transport, bound Compton scattering and photo-electrons from K, L, and M shells are considered for all energies. In both cases, resulting fluorescence or Auger and Coster-Kronig electrons are followed. The input data for photon cross sections have been updated by Seuntjens et al. (2002), who used the XCOM database (Berger and Hubbell, 1987) to improve the cross sections for the photoelectric effect, Rayleigh scattering, and pair production. Radiative Compton corrections in the one-loop approximation based on the Brown and Feynman equation (1952) are applied. However, the effect of reducing the cross section for large scattering angles is

partially cancelled by the inclusion of double-Compton events. For the pair-production cross section, cross sections in EGS4 are employed following the techniques of Øverbø et al. (1973). In this report, photon transport is terminated when the photon energy falls below 2 keV.

(27) Electron transport calculations are performed by a Class II condensed history technique (Berger, 1963), which transports secondary particles produced above a certain chosen energy. Bremsstrahlung cross sections agree with those of the National Institute of Standards and Technology (NIST) database (Seltzer and Berger, 1985, 1986), which in turn form the basis for the radiative stopping powers recommended by the International Commission on Radiation Units and Measurements (ICRU, 1984). Electron impact ionisation is modelled using default cross sections (Kawrakow, 2002). For elastic scattering, spin effects are taken into account. Pair production is simulated as in EGS4 (Nelson et al., 1985). Triplet-production processes are neglected for all particles. In this report, the transport history of electrons is generally terminated when their kinetic energy falls below 20 keV. Exceptions are noted for electrons with an initial kinetic energy below 50 keV, whose histories are followed down to 2 keV. A variance reduction technique called ‘bremsstrahlung splitting’ was employed to decrease the relative statistical uncertainty in the dose conversion coefficients of internal organs (Kawrakow et al., 2009).

(28) Representative plots of photon and electron SAFs are shown below in Figs. 2 to 6. For each source and target region combination, the photon SAFs are shown in the upper panel of each figure, with the electron SAFs shown in the lower panel.

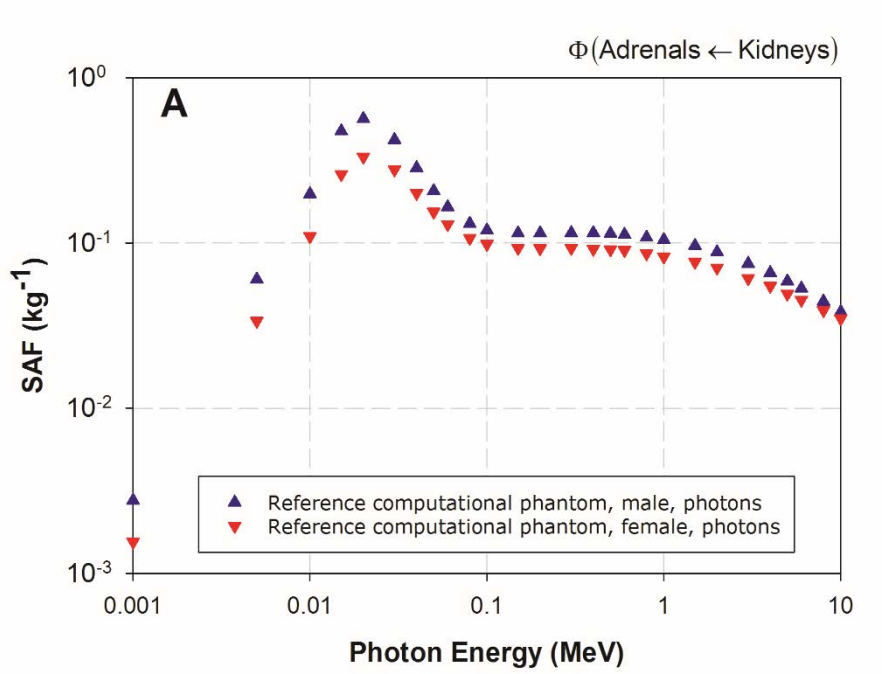

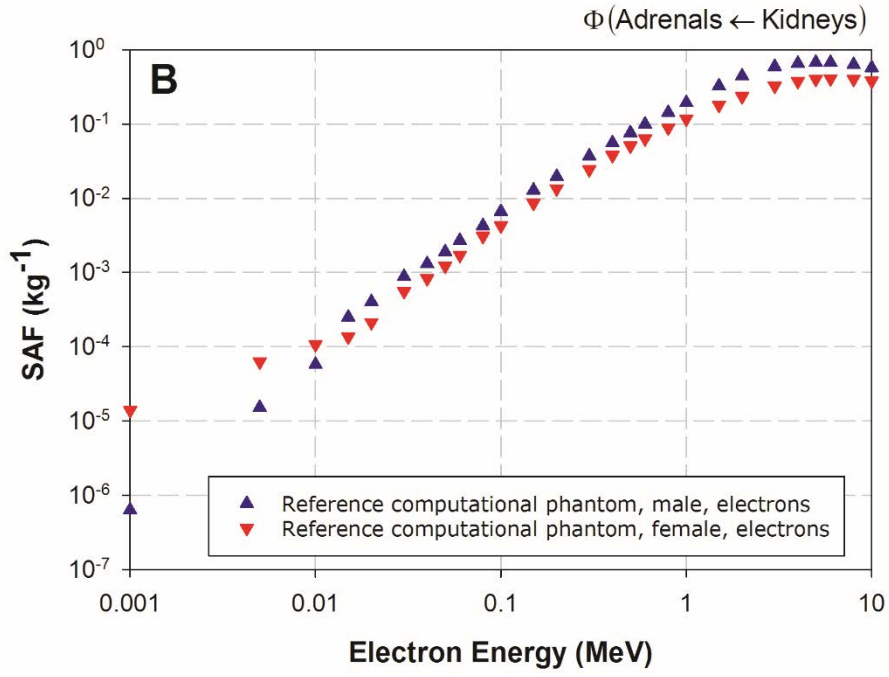

Fig. 2. SAFs to the adrenal glands within the reference adult male and reference adult female corresponding to uniformly distributed monoenergetic photon (A) and electron (B) sources in the kidneys.

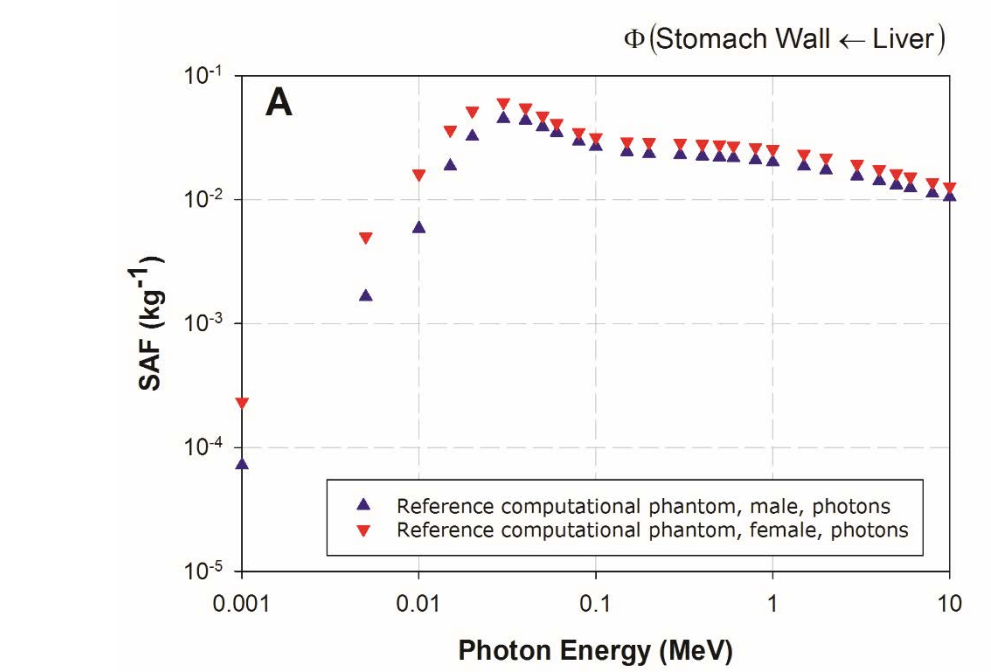

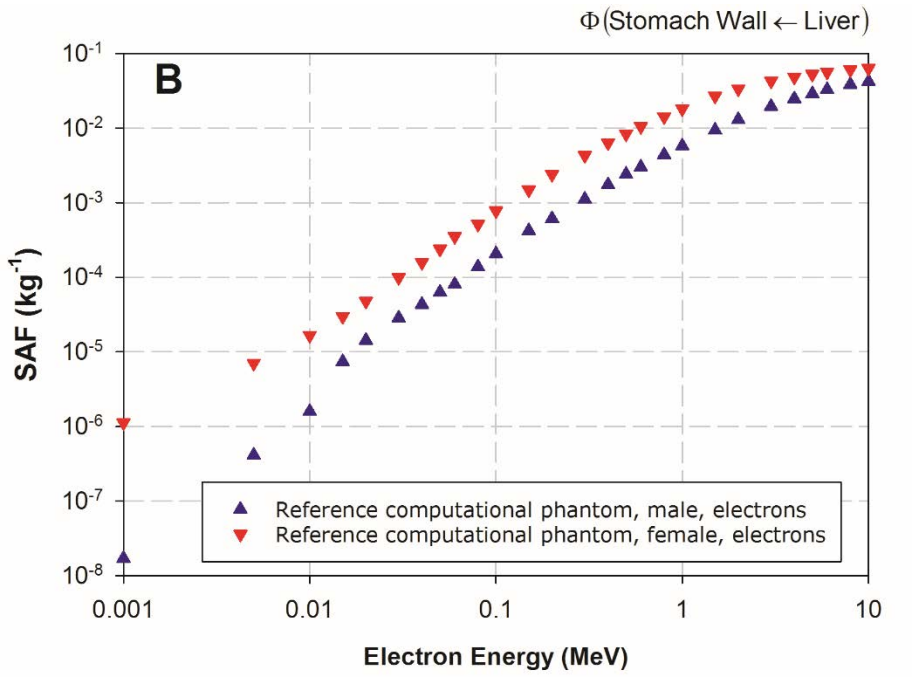

Fig. 3. SAFs to the stomach walls within the reference adult male and reference adult female corresponding to uniformly distributed monoenergetic photon (A) and electron (B) sources in the liver.

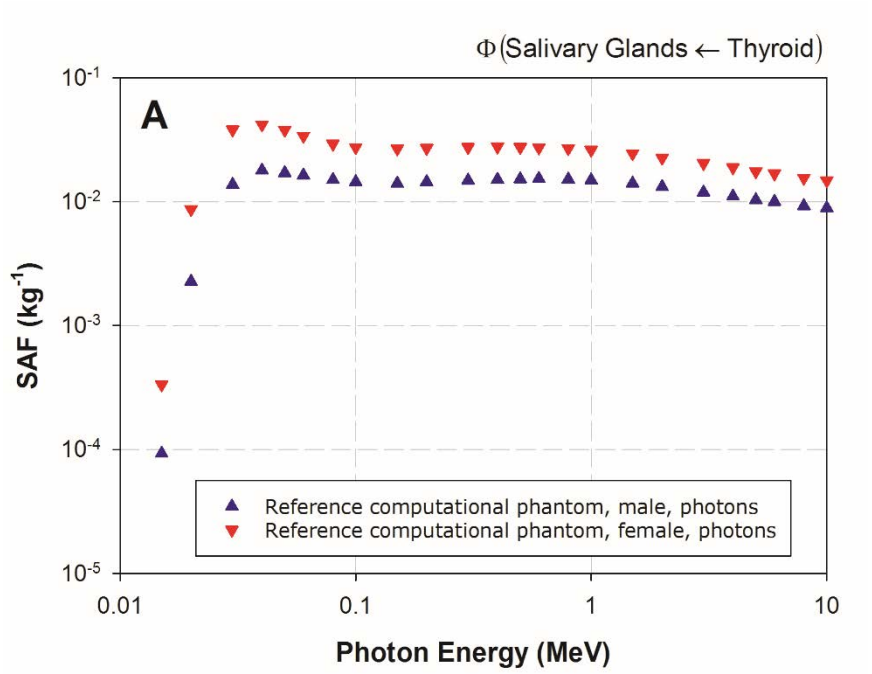

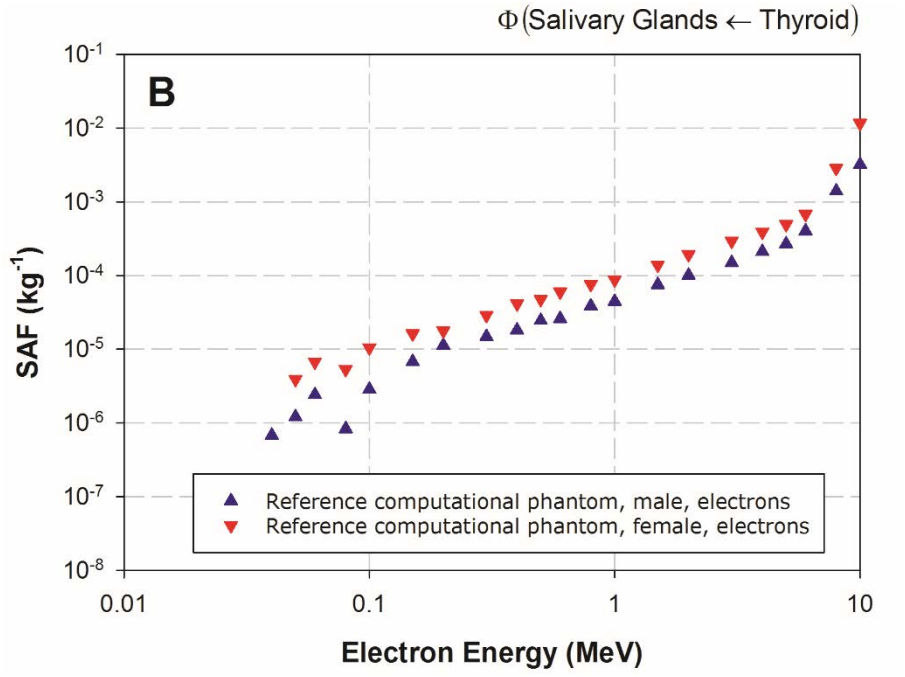

Fig. 4. SAFs to the salivary glands within the reference adult male and reference adult female corresponding to uniformly distributed monoenergetic photon (A) and electron (B) sources in the thyroid.

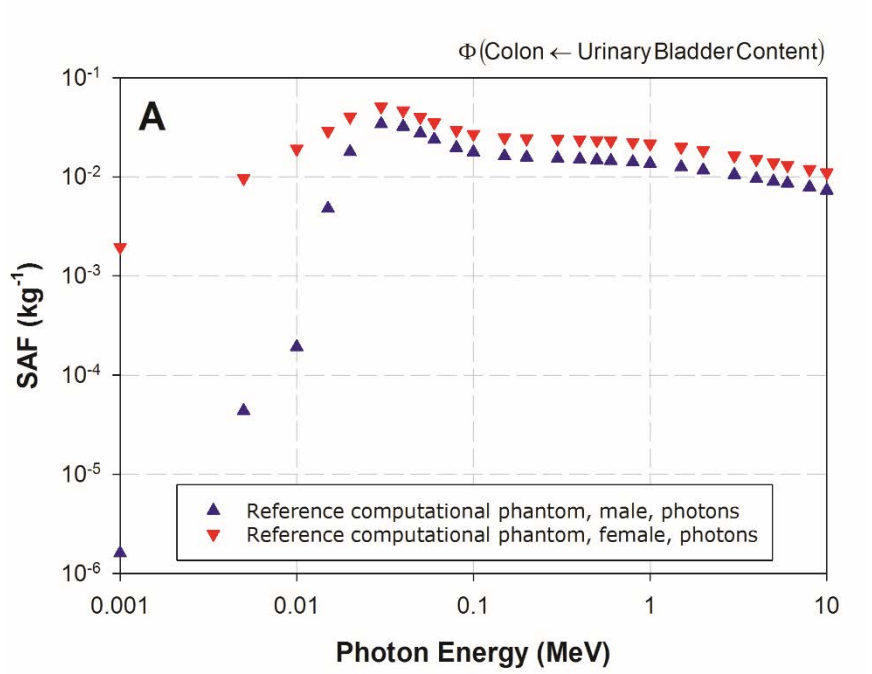

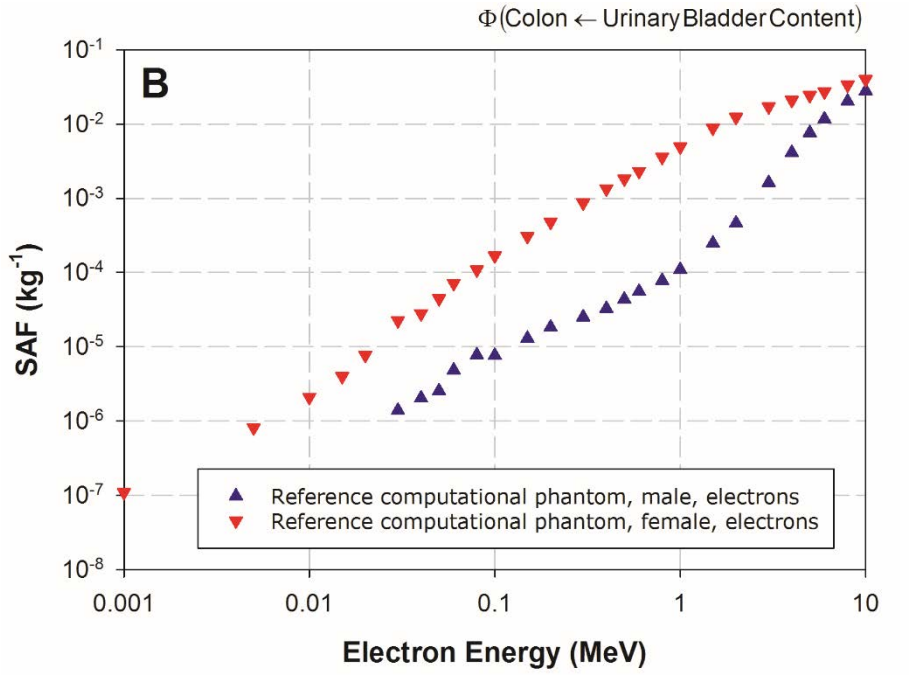

Fig. 5. SAFs to the colon wall within the reference adult male and reference adult female corresponding to uniformly distributed monoenergetic photon (A) and electron (B) sources in the urinary bladder contents.

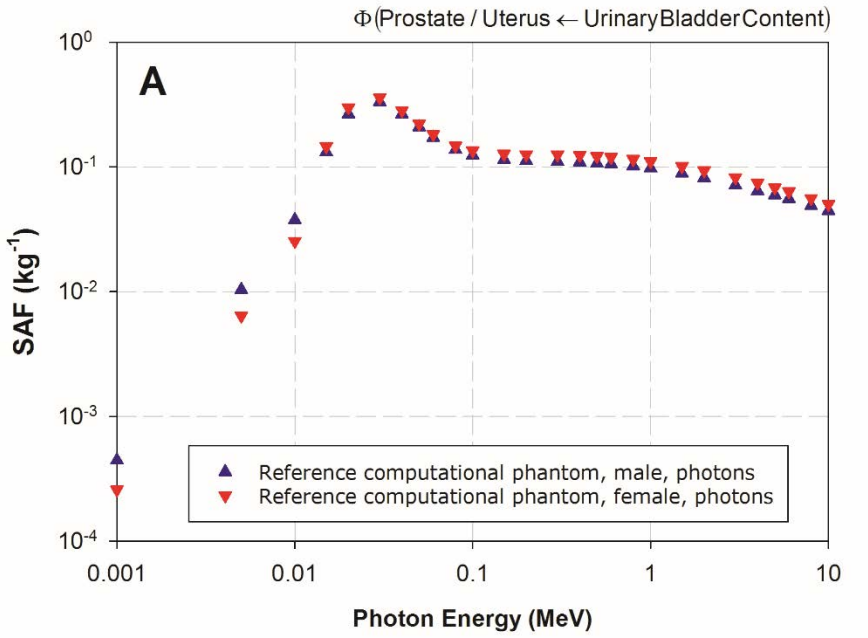

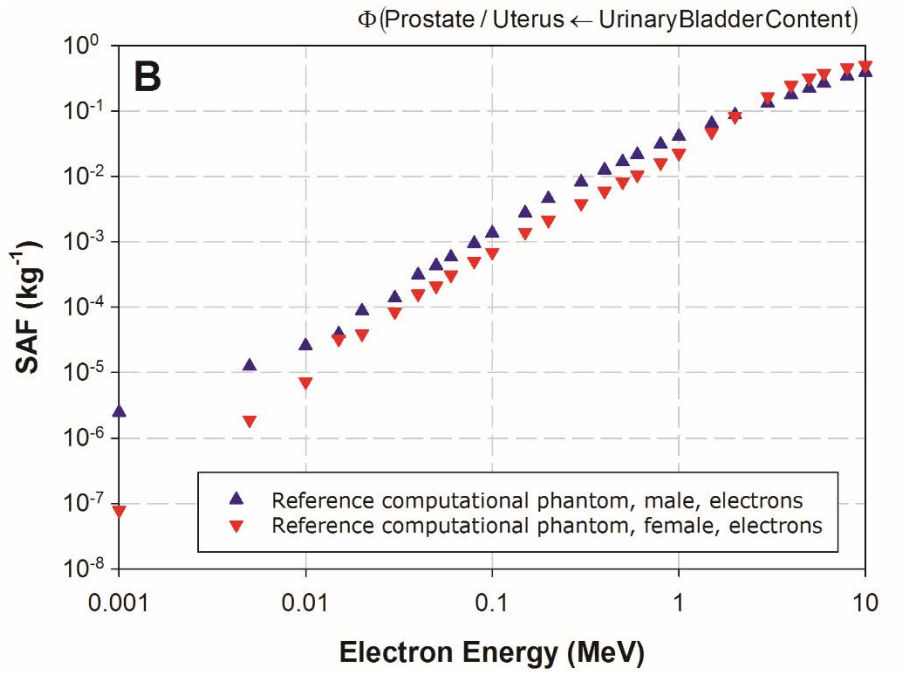

Fig. 6. SAFs to the prostate gland within the reference adult male and the uterus within the reference adult female corresponding to uniformly distributed monoenergetic photon (A) and electron (B) sources in the urinary bladder contents.

3.2.2. Neutron transport calculations

(29) For calculations of neutron absorbed fraction, the Los Alamos National Laboratory Monte Carlo radiation transport code Monte Carlo N-Particle eXtended (MCNPX) Version 2.6.0 has been used (Pelowitz 2008). MCNPX is capable of tracking many particle types over broad energy ranges.

(30) The transport of neutrons, photons and electrons below 20 MeV is the same as in the MCNP4C3 code, and is simulated using continue-energy nuclear, photoatomic, and electron data libraries. Data libraries used for neutrons, photons, and electrons are ENDF/B-VI, mcplib04, and el03, respectively. Thermal neutron scattering is strongly dependent on the molecular binding energy of hydrogen. This effect is taken into account by using $S(\alpha, \beta)$ data for hydrogen in water.

(31) In this report, values for neutron absorbed fraction were calculated for neutrons from spontaneous fission having wide energy distribution expressed by the Watt spectrum (ICRP, 2008). In the energy range considered in the present calculation (<20 MeV), there are four main ways in which neutrons interact with human tissue, namely, neutron capture, elastic scattering, inelastic scattering and nuclear reactions. In the lower energy region, neutron capture is dominant although the cross section usually decreases with the inverse square root of the neutron energy. The 2.2 MeV photons, which are emitted by the capture of thermalised neutrons in hydrogen via the $^{1}H(n, \gamma)^{2}D$ reaction, play a significant role in the deposition of energy in the human body. The $^{14}N(n, p)^{14}C$ reaction, which produces protons of ~ 600 keV, also contributes to the absorbed dose. At energies above ~1 keV, the energy deposited by recoil protons from elastic scattering by hydrogen atoms becomes significant. Inelastic scattering is reactions with energy thresholds in which the neutron loses energy, exciting the nucleus to emit photons without the emission of charged particles. At most, inelastic scattering contributes only to a small percent of the total absorbed doses in body tissue. At energies above a few MeV, the production of charged particles by nuclear reactions [(n, D), (n, T), (n, α), etc.] becomes an increasingly significant mechanism for the deposition of energy.

3.3. Sampling algorithms for distributed organs and tissues

(32) For sampling points in different source regions, there are several cases to be considered.

3.3.1. Sampling algorithm A

(33) The simplest situation is a single organ that is located at a specific position in the body such as the brain, liver, pancreas, or spleen. The most straightforward sampling method is then the following sampling algorithm.

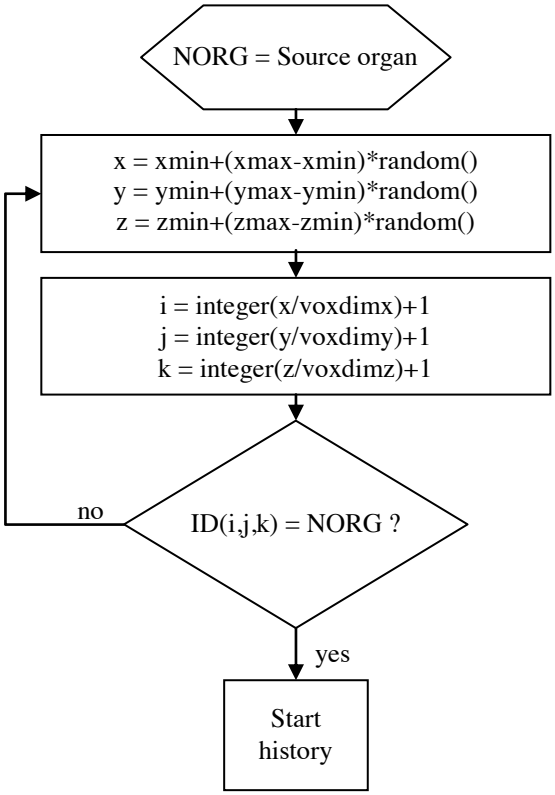

Fig. 7. Schematic of sampling algorithm A.

3.3.2. Sampling algorithm B

(34) If a source region is distributed throughout the body such as muscle, sampling algorithm A may lead to a large proportion of rejected points. In this case, it may be better to use the following sampling algorithm.

(35) Let N be the number of voxels belonging to the region in question. These voxels are collected in a separate (N,3)-dimensional array NPOS. The value stored at NPOS(m,1) is the column, NPOS(m,2) is the row and NPOS(m,3) the slice where the m^{th} voxel of the source region is located. To select a voxel, one multiplies N with a random number from the interval (0,1). The nearest integer number above this product is then used to identify a source voxel in the NPOS array. Then x, y and z co-ordinates are sampled independently inside the selected voxel. All sampled co-ordinate points can be used.

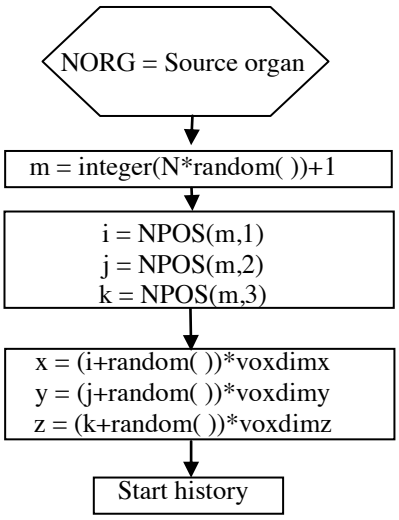

Fig. 8. Schematic of sampling algorithm B.

(36) In case the voxel number N of a source region is very large, there is a trade-off between wasted CPU time (in case of sampling algorithm A) and large storage requirement (sampling algorithm B). Selecting between these algorithms is at the discretion of the user.

3.3.3. Sampling algorithm C

(37) A further common situation is that of an organ pair where both organs are small, but they are relatively distant from each other, such as the adrenals. An efficient sampling algorithm may then be the following which is a combination of schemes A and B.

(38) Let Nl be the number of voxels belonging to the left one of an organ pair, Nr the number of voxels belonging to the right one, N=Nl+Nr the sum of both, and rl=Nl/N the ratio of the voxel number of the left organ to that of both organs. If a sampled random number r is smaller than rl, a source point is sampled according to algorithm A in the left organ, otherwise it is sampled in the right organ. This sampling algorithm can be extended to organ groups consisting of more than two parts.

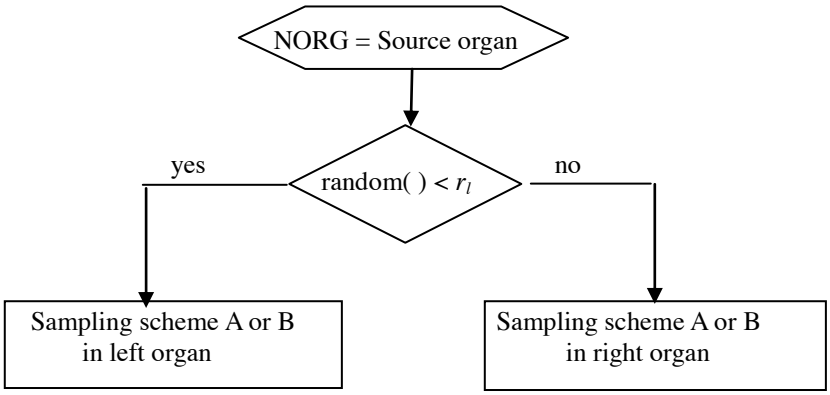

Fig. 9. Schematic of sampling scheme C.

3.3.4. Sampling algorithm D

(39) The sampling algorithms mentioned above are for sources distributed homogeneously in the volume of an organ or organ group. There are, however, situations where inhomogeneous source distributions have to be considered. For example, consider a source uniformly distributed in trabecular bone which is not uniquely identified but is included within spongiosa. The same algorithm is equally applicable to marrow sources. There are mainly two recommended approaches.

(40) In this algorithm, the entirety of the segmented spongiosa voxels of all bones serves as volume in which one samples source points for particle emissions (using schemes A or B). However, since the relative amount of trabecular bone in the spongiosa varies between individual bones and bone groups, the source cannot be assumed as homogeneously distributed in volume. Therefore, the relative amount of trabecular bone in the segmented spongiosa volume of each specific bone or bone group is used as rejection criterion for accepting source points. Let $r_{t,b}$ be the relative amount of trabecular bone in the spongiosa of bone (group) b [respective data derived from Tables 3 and 4 in Zankl et al. (2005), see Table 4]. If a sampled random number r is smaller than $r_{t,b}$, the source point is accepted, otherwise rejected.

(41) This sampling algorithm is not optimal, since for each bone constituent and each spongiosa region, there is a nonzero probability of rejecting a sampled source point. Therefore, these data are normalised to the maximum value of each constituent among all spongiosa regions in Table 5. For the spongiosa region with the highest proportion of the respective bone constituent, all sampled source points are accepted; for all other spongiosa regions, the probability of rejection is reduced.

Table 4. Mass ratios of bone constituents (trabecular bone, red bone marrow, yellow bone marrow) in the spongiosa regions of the reference computational phantoms.

Spongiosa region	Male			Female		
	Bone	RBM	YBM	Bone	RBM	YBM
Humeri, upper half	0.303	0.146	0.234	0.307	0.185	0.350
Humeri, lower half	0.195	0.000	0.600	0.230	0.000	0.652
Ulnae, radii (lower arm bones)	0.195	0.000	0.600	0.230	0.000	0.652
Hand bones	0.195	0.000	0.600	0.230	0.000	0.652
Clavicles	0.236	0.176	0.341	0.316	0.178	0.344
Skull (cranium)	0.242	0.197	0.306	0.385	0.164	0.255
Femora, upper half	0.202	0.166	0.419	0.094	0.268	0.589
Femora, lower half	0.195	0.000	0.600	0.230	0.000	0.652
Tibiae, fibulae, patellae	0.195	0.000	0.600	0.230	0.000	0.652
Foot bones	0.195	0.000	0.600	0.230	0.000	0.652
Mandible (facial skeleton)	0.330	0.127	0.197	0.311	0.208	0.322
Pelvis (os coxae)	0.189	0.301	0.311	0.186	0.354	0.365
Ribs	0.239	0.363	0.148	0.141	0.559	0.228
Scapulae	0.276	0.170	0.265	0.222	0.260	0.404
Cervical spine	0.062	0.620	0.253	0.213	0.482	0.197
Thoracic spine	0.101	0.563	0.229	0.127	0.574	0.234
Lumbar spine	0.161	0.476	0.194	0.267	0.424	0.173
Sacrum	0.029	0.668	0.272	0.071	0.634	0.259
Sternum	0.046	0.644	0.263	0.114	0.588	0.240

Table 5. Normalised mass ratios of bone constituents (trabecular bone, red bone marrow, yellow bone marrow) in the spongiosa regions. Compared to the data of Table 4, the entries of each column have been divided by the maximum entry in the respective column.

Spongiosa region	Male			Female		
	Bone	RBM	YBM	Bone	RBM	YBM
Humeri, upper half	0.916	0.218	0.391	0.799	0.292	0.538
Humeri, lower half	0.591	0.000	1.000	0.599	0.000	1.000
Ulnae, radii (lower arm bones)	0.591	0.000	1.000	0.599	0.000	1.000
Hand bones	0.591	0.000	1.000	0.599	0.000	1.000
Clavicles	0.713	0.264	0.568	0.822	0.281	0.528
Skull (cranium)	0.734	0.295	0.510	1.000	0.258	0.391
Femora, upper half	0.613	0.249	0.699	0.246	0.422	0.904
Femora, lower half	0.591	0.000	1.000	0.599	0.000	1.000
Tibiae, fibulae, patellae	0.591	0.000	1.000	0.599	0.000	1.000
Foot bones	0.591	0.000	1.000	0.599	0.000	1.000
Mandible (facial skeleton)	1.000	0.190	0.328	0.808	0.327	0.495

Pelvis (os coxae)	0.574	0.451	0.518	0.484	0.558	0.560
Ribs	0.723	0.544	0.247	0.366	0.882	0.350
Scapulae	0.835	0.255	0.441	0.578	0.410	0.620
Cervical spine	0.187	0.929	0.422	0.553	0.760	0.302
Thoracic spine	0.307	0.843	0.383	0.331	0.904	0.359
Lumbar spine	0.487	0.714	0.324	0.694	0.668	0.265
Sacrum	0.089	1.000	0.454	0.184	1.000	0.397
Sternum	0.138	0.965	0.438	0.295	0.928	0.368

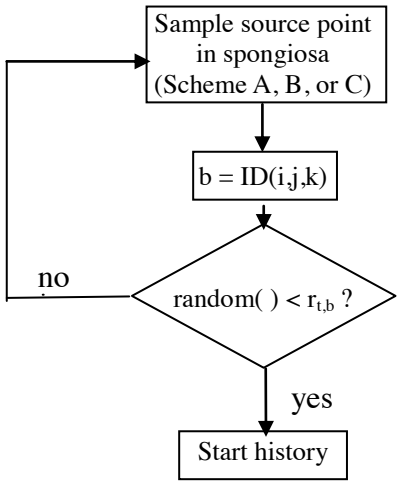

Fig. 10. Schematic of sampling algorithm D.

3.3.5. Sampling algorithm E

(42) As with algorithm D, the whole spongiosa is taken as the volume from which source points can be sampled. In contrast to algorithm D, however, $r_{t,b}$, the relative amount of trabecular bone in the spongiosa of bone (group) b, is not used as criterion to accept or reject a source point, but each particle starting in the spongiosa volume is assigned this value as its initial "statistical weight".

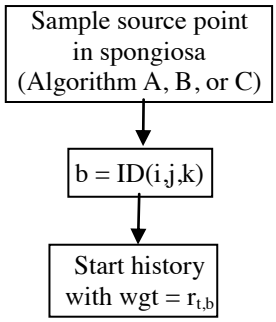

Fig. 11. Schematic of sampling algorithm E.

(43) Sampling algorithm E is also recommended when the source is the whole body. Since homogeneous sources in the whole body should be considered to be distributed homogeneously by mass (not by volume), source points can be sampled uniformly in the whole body volume, and then the density of the organ/tissue where a source point is located can be assigned as statistical weight to the starting particle history.

(44) Another inhomogeneous source distribution arises when the source is the blood. The larger blood vessels have been segmented directly; here, the entire volume is blood source. However, the blood distribution inside the organs has been considered by including a respective proportion of blood in the tissue composition of each organ. Therefore, when a blood source has to be sampled, each organ contributes with the fraction of its mass that is due to blood. The blood fractions of the different tissues are given in Table 6. In this case, again either sampling algorithm D or sampling algorithm E is recommended.

Table 6. Mass fraction of blood in the different body tissues.

No.	Medium	Blood fraction	
		Male	*Female*
1	Teeth	0.000	0.000
2	Mineral bone	0.010	0.010
3	Humeri, upper half, spongiosa	0.054	0.060
4	Humeri, lower half, spongiosa	0.024	0.025
5	Lower arm bones, spongiosa	0.024	0.025
6	Hand bones, spongiosa	0.024	0.025
7	Clavicles, spongiosa	0.057	0.059
8	Cranium, spongiosa	0.061	0.060
9	Femora, upper half, spongiosa	0.053	0.015
10	Femora, lower half, spongiosa	0.024	0.025
11	Lower leg bones, spongiosa	0.024	0.025
12	Foot bones, spongiosa	0.024	0.025
13	Mandible, spongiosa	0.052	0.064
14	Pelvis, spongiosa	0.077	0.018
15	Ribs, spongiosa	0.090	0.013
16	Scapulae, spongiosa	0.058	0.068
17	Cervical spine, spongiosa	0.127	0.105
18	Thoracic spine, spongiosa	0.119	0.117
19	Lumbar spine, spongiosa	0.106	0.098
20	Sacrum, spongiosa	0.134	0.124
21	Sternum, spongiosa	0.131	0.118
22	Humeri and femora, upper halves, medullary cavity	0.015	0.014
23	Humeri and femora, lower halves, medullary cavity	0.015	0.014
24	Lower arm bones, medullary cavity	0.015	0.014
25	Llower leg bones, medullary cavity	0.015	0.014
26	Cartilage	0.015	0.014
27	Skin	0.051	0.054

28	Blood	1.000	1.000
29	Muscle tissue	0.027	0.025
30	Liver	0.311	0.293
31	Pancreas	0.240	0.205
32	Brain	0.046	0.038
33	Heart	0.027	0.025
34	Eyes	0.170	0.144
35	Kidneys	0.361	0.298
36	Stomach	0.295	0.234
37	Small intestine	0.327	0.260
38	Large intestine	0.333	0.251
39	Spleen	0.523	0.442
40	Thyroid	0.168	0.145
41	Urinary bladder	0.022	0.021
42	Testes / ovaries	0.064	0.075
43	Adrenals	0.240	0.189
44	Oesophagus	0.295	0.234
45	Gallbladder, pituitary gland, trachea, thymus, tonsils, ureters, ...	0.170	0.144
46	Prostate / uterus	0.170	0.144
47	Lymph	0.015	0.014
48	Breast (mammary gland)	0.170	0.144
49	Adipose tissue	0.019	0.018
50	Lung tissue (compressed lungs)	0.417	0.388
51	Gastro-intestinal tract - contents	0.000	0.000
52	Urine	0.000	0.000
53	Air	0.000	0.000

(45) The variables used in the above schematics that have not been explained in the text are the following:

ID(i,j,k)	the 3D voxel array of organ identification numbers
Voxdimx	voxel dimension in x direction (column width)
Voxdimy	voxel dimension in y direction (row depth)
Voxdimz	voxel dimension in z direction (slice height)
xmin	minimum x co-ordinate of the rectangular prism containing the organ in question
xmax	maximum x co-ordinate of the rectangular prism containing the organ in question
ymin	minimum y co-ordinate of the rectangular prism containing the organ in question
ymax	maximum y co-ordinate of the rectangular prism containing the organ in question
xmin	minimum x co-ordinate of the rectangular prism containing the organ in question
xmax	maximum x co-ordinate of the rectangular prism containing the organ in question
random( )	random number with values in the interval (0,1)
wgt	initial statistical weight of particle history (wgt = 1, if not specified otherwise)

4. COMPUTATIONAL METHODS FOR THE SKELETAL TISSUES

(46) For radiological protection purposes, the Commission defines two skeletal cell populations of dosimetric interest relevant to stochastic biological effects: (i) haematopoietic stem cells associated with the risk of radiogenic leukaemia, and (ii) osteoprogenitor cells associated with the risk of radiogenic bone cancer. While data now show that haematopoietic stem cells are found preferentially near the surfaces of the bone trabeculae within skeletal spongiosa (Watchman et al., 2007; Bourke et al., 2009), current modelling for radiological protection assumes these cells to be uniformly distributed within the marrow cavities of haematopoietically active marrow. For the osteoprogenitor cells, the Commission had previously defined their location as a single cell layer within trabecular and cortical endosteum, each 10 μm in thickness, and located along the surfaces of the bone trabeculae and Haversian canals, respectively (ICRP, 1977). In *Publication 110* (ICRP, 2009), the surrogate target tissue for the osteoprogenitor cells was redefined as being 50 μm in thickness along the surfaces of the bone trabeculae in skeletal spongiosa, and along the inner surfaces of the medullary cavities in the shafts of all long bones. As a result, cortical bone and its cells within the Haversian canals are no longer considered to be a target tissue for dose assessment. In this report, the revised 50 μm surrogate target tissue for the osteoprogenitor cells is termed the 'endosteum' and is given the symbol TM_{50} (total marrow within a 50-mm thickness of the bone surfaces). The term 'bone surfaces' is no longer used to describe the target cell layer of relevance to radiogenic bone cancer.

(47) Neither of these skeletal target tissues at radiological risk can be geometrically represented within the voxel structure of the ICRP reference phantoms. As presented above, the skeleton in the male and female reference computational phantoms is described by voxels defining either cortical bone, medullary marrow, or trabecular spongiosa. The latter is a homogeneous mixture of its microscopic tissue constituents – bone trabeculae, active marrow, and inactive marrow – and thus varies in both elemental composition and mass density across different bones of the skeleton in each reference phantom. Computational algorithms must therefore be applied to relate the absorbed dose to spongiosa and medullary marrow to the absorbed dose to either active marrow or endosteum. The elemental compositions of the constituent tissues of trabecular spongiosa are given in Table 3.1 of *Publication 116* (ICRP, 2010). It is further noted that the elemental composition of endosteum is equal to that of the active marrow/inactive marrow mixture in a particular skeletal site as determined by its reference marrow cellularity given in *Publication 70* (ICRP, 1995).

4.1. Models for electron transport

(48) Computations of SAFs for charged particles originating within the skeletonal tissues require detailed geometrical data on both (i) the bone macrostructure (i.e. regions of spongiosa, cortical bone, and medullary marrow), and (ii) the bone microstructure (i.e. regions of trabecular bone, active bone marrow, and inactive bone marrow). While the former can be properly modelled with the structure of the *Publication 110* reference computational phantoms, the latter requires additional geometrical data for radiation transport within the trabecular spongiosa. In this report,

the microCT imaging data of Hough et al. (2011) were used for radiation transport simulation in 38 cored samples of spongiosa imaged under microCT at an isotropic resolution of 30 μm. The radiation transport code EGSnrc was used under Paired-Image Radiation Transport to follow individual electrons simultaneously through both the 3D geometry of ex-vivo CT images of the harvested bone sites and the 3D geometry of the segmented microCT images of spongiosa (Hough et al., 2011). Marrow voxels of the latter were randomly tagged as either active or inactive marrow to achieve reference cellularities for each bone site. Radiation transport results were reported as absorbed fractions for electrons over the energy range of 1 keV to 10 MeV. Source regions included bone marrow (both active and inactive), trabecular bone (both volumes and surfaces), and cortical bone (both volumes and surfaces). The method utilised in Hough et al. (2011) (i) explicitly accounts for electron escape from spongiosa, (ii) explicit consideration of spongiosa cross-fire from cortical bone, and (iii) the revised 50-μm thickness of the endosteum target for bone cancer risk. SAF values reported in this report are ratios of the absorbed fractions calculated in Hough et al. (2011), and reference skeletal tissue masses for the ICRP Reference Adult Male and Reference Adult Female as defined in *Publication 110*.

4.2. Models for recoil proton transport following neutron interactions

(49) Computations of absorbed fractions of energy for recoil protons originating in the skeleton have been performed using linear pathlength techniques. These techniques were first developed and described by the Spiers' group (Beddoe et al., 1976; Beddoe and Spiers, 1979; Spiers and Beddoe, 1977; Spiers et al., 1978a,b, 1981; Whitwell and Spiers, 1976; Darley, 1972; Spiers, 1968; Whitwell, 1973), subsequently refined by Eckerman and Stabin (2000) and Bouchet et al. (1999), and most recently revisited by Jokisch et al. (2011a,b). This method was also the basis for recoil proton absorbed fractions used in neutron dose response functions as summarised in Annex E of *Publication 116* (ICRP, 2010). Distributions of linear pathlength segments across trabecular bone and marrow (inclusive of all soft tissue components) were obtained from the high resolution microCT images via digital measurements techniques described in Rajon and Bolch (2003) and Rajon et al. (2002) and published for the 40 year old male cadaver (Jokisch et al. 2011b).

(50) These two pathlength distributions for a given skeletal site were then utilised in an algorithm (Jokisch et al. 2011a, b) that uses the continuous slowing down approximation (CSDA) range of the charged particle of interest to compute fractional energy deposition in the various skeletal tissues. This algorithm includes a basis for dividing the total marrow space (TMS) into active (AM) and inactive (IM) components based on typical sizes of skeletal adipose (Reverter et al. 1993). The endosteum (TM_{50}) portion of the TMS pathlength is determined via an algorithm developed by Jokisch et al. (2011a).

(51) Range/energy data for protons utilising the CSDA were obtained from ICRU Report 49 (1993). Bragg-Kleeman scaling techniques described in Tsoulfanidis (1983) were utilised to convert ICRU Report 49 Water to ICRU Report 46 (1992) Adult Red Marrow (used for AM) and Adult Yellow Marrow (used for IM). ICRU

Report 49 Compact Bone was scaled to yield data for ICRU Report 46 Adult Cortical Bone (TBV).

(52) When multiple trabecular cores comprise a single skeletal site, a source mass-weighted average absorbed fraction, of the constituent samples, x, was computed as

$$\phi_{site}\left(r_T \leftarrow r_S\right) = \sum_x \frac{m_{x,S}}{m_{site,S}} \phi_x\left(r_T \leftarrow r_S\right) \tag{4.1}$$

where $\frac{m_{x,S}}{m_{site,S}}$ is the fraction of total site source mass in sample x. Note that this method was also utilised to compute a skeletal averaged absorbed fraction using results from all skeletal sites.

4.3. Models for alpha particle transport

(53) Computations of SAFs of energy from alpha particles (2.0-12.0 MeV) originating in the skeleton were performed using three models: (1) the pathlength-based CSDA model described in paragraphs 49 and 50 but adapted for alpha particles; (2) a model performing CSDA range-based transport in voxelised images; and (3) a model using MCNPX (Waters, 2002; Pelowitz, 2008) alpha particle transport in voxelised images.

(54) The first two models utilised identical CSDA range/energy data but differ slightly in their input geometry. While they both utilised data from the same 40 year male cadaver, the second model used the 3D voxelised image for the transport geometry whereas the first model utilised pathlength distributions obtained from those images. The second and third models used identical transport geometries (the voxel image) but differ in the radiation transport (CSDA compared MCNPX). As a result of the difference in geometry input, the pathlength model also differs slightly from the voxel models in the modeling of the endosteum target (TM_{50}), inactive marrow constituent (IM), and the algorithm for modeling radiation originating on the trabecular bone surface (TBS).

(55) These differences form the basis for the recommended use of one model over another, or the averaging the results of two models for particular source/target combinations. For alpha particles originating in the active marrow irradiating the active marrow (AM←AM), the pathlength model was utilised since it is thought to have a more realistic modeling of the inactive marrow constituent. For a surface source irradiating the active marrow (AM←TBS), the CSDA voxel model was utilised since it has a marrow cellularity near the surface consistent with the cellularity of the entire marrow space. For the same reason, the CSDA voxel model was also utilised for alpha particles originating in the active marrow irradiating the endosteum (TM_{50}←AM). For the remaining endosteum (TM_{50}) target geometries, an average of the pathlength and voxel model results were used, as differences were observed but no basis for preference was determined. Finally, for the remaining active

marrow (AM) target geometries, no significant differences were observed between the models.

4.4. Response functions for photon and neutron dose to the skeletal tissues

(56) As noted above, the tissues of the skeleton at radiological risk, and hence assigned tissue weighting factors w_T, cannot be represented geometrically in the ICRP reference computational phantoms. The energy deposition in these tissues is influenced by their proximity to those of different densities and elemental compositions. This energy deposition can, however, be derived during the Monte Carlo calculations of photon transport through scaling the calculated photon fluence in different skeletal regions (spongiosa or medullary cavities) by functions representing the absorbed dose to the target tissue per photon (Eckerman, 1985; Eckerman et al., 2008; Johnson et al., 2011) or neutron fluence (Bahadori et al., 2011). These functions, referred to as response functions $\mathcal{R}$, are derived using models of the microscopic structure of bone geometry of different skeletal regions and the transport of the secondary ionising radiations through those geometries. For photons, these secondary radiations are electrons and positrons whose absorbed fractions within the skeletal tissues were developed in Hough et al. (2011). For neutrons, these secondary radiations are several, but most importantly recoil protons owing to their lower linear energy transfer (LET) and thus longer range within trabecular spongiosa (Jokisch et al., 2011a). In this work, all photon SAFs for target regions in the skeleton were derived using EGSnrc tabulations of energy-dependent photon fluence and photon skeletal dose response function presented in Annex D of *Publication 116* (ICRP, 2010). Similarly, all neutron SAFs for target regions in the skeleton were derived using MCNPX tabulations of energy-dependent neutron fluence and neutron skeletal dose response functions presented in Annex E of *Publication 116* (ICRP, 2010).

5. COMPUTATIONAL METHODS FOR THE RESPIRATORY TRACT

(57) Many of the electron and alpha particle absorbed fractions (AFs) tabulated in Appendix H of *Publication 66* (ICRP, 1994) for the respiratory tract were adopted directly in this document, with the following exceptions:

(i) revisions to the respiratory tract particle transport model (ICRP, 2015) required changes in dosimetric assumptions regarding the bronchial and bronchiolar regions; and

(ii) *Publication 66* electron SAFs were augmented with selected values from the reference computational phantoms in cases where the absorbed fractions had previously been assumed to be either unity or zero.

(58) Revisions in the structure of the HRTM, in particular to the particle transport model in the bronchial (BB) and bronchiolar (bb) regions, meant that the dosimetric model for these sources had to be reconsidered. The original HRTM included particle size-dependent slow clearance compartments, BB2 (bronchial) and bb2 (bronchiolar). Material that cleared rapidly from these regions was represented by corresponding compartments BB_1 and bb_1. Activity associated with the slow compartments was assumed to be distributed within the ciliated sol layer adjacent to the airway walls and activity in the fast compartments was taken to be dispersed throughout the mucous gel overlaying the sol (ICRP, 1994). The size-dependent slow clearance compartments were eliminated in the revised HRTM (ICRP, 2015) leaving a single phase of clearance in both regions. Because of uncertainty in the location relative to the target cells within the airway walls, of the activity being cleared in mucus, due to factors including uncertainties in the values of the mean thicknesses of the two mucous layers, activity in the revised BB and bb compartments is taken to be uniformly distributed throughout both the gel and sol layers. The absorbed fractions for the new single phase of clearance are weighted averages of those for the original fast (gel) and slow (sol) compartments. The weights are the relative thicknesses of the gel and sol layers, 5/11 and 6/11, respectively, for the bronchial region BB, and 2/6 and 4/6 for the bronchiolar region bb (ICRP, 1994). Thus, the revised electron and alpha particle absorbed fractions for bronchial and bronchiolar surface sources are given by:

$$\phi(r_T \leftarrow BB) = \left(\frac{5}{11}\right)\phi(r_T \leftarrow BB_1) + \left(\frac{6}{11}\right)\phi(r_T \leftarrow BB_2) \tag{5.1}$$

$$\phi(r_T \leftarrow bb) = \left(\frac{2}{6}\right)\phi(r_T \leftarrow bb_1) + \left(\frac{4}{6}\right)\phi(r_T \leftarrow bb_2) \tag{5.2}$$

where r_T denotes the appropriate target tissue.

(59) The *Publication 66* electron SAFs were supplemented with extra cross-fire terms (when AF = 0) or improved self-dose values (when AF = 1) derived from electron transport calculations in the male and female reference computational

phantoms. For many organs in the reference phantoms, the SAFs computed for self-irradiation were approximately inversely proportional to mass with only minor or moderate deviations from mass scaling. This could be exploited in instances of self irradiation in the HRTM where target cells are located accurately in the phantom but with inadequate voxel resolution by correcting the SAFs with the reference mass. This applied to alveolar-interstitial and extrathoracic lymph node sources, replacing the original default assumption that AF = 1 for these cases and allowing for energy-dependent electron escape.

(60) Electron cross-fire SAFs for many source and target combinations exhibited reciprocity over wide energy ranges, implying that the cross-fire SAFs were independent of source or target masses and did not require mass correction. Consequently, selected values could be used directly to fill any vacancies in the HRTM SAF matrix where cross-fire absorbed fractions had previously been assumed to be zero at all energies.

(61) Alpha particle SAFs were not supplemented in this fashion. The electron and alpha particle absorbed fractions that were adopted from *Publication 66* were assumed to be gender-independent, but the SAFs derived from them used male or female target masses as appropriate. For consistency, the derived values were mapped onto the energy grid used for reference phantom radiation transport calculations.

6. COMPUTATIONAL METHODS FOR THE ALIMENTARY TRACT

(62) In *Publication 100*, the morphometric and dosimetric models of the alimentary tract are defined, including source regions of radionuclide deposition and target regions of radiosensitive stem cells. For electron sources in the alimentary tract, Annex F of *Publication 100* provided provisional values of SAFs based upon Monte Carlo radiation transport simulation in the geometric models of that report. Alpha particle transport was not considered in *Publication 100*, and thus values of SAF of alpha emissions presumed full energy deposition in the source region.

(63) In the present report, new radiation transport simulations were performed for both electron and alpha particle sources using the geometric models described in Section 7.2 of *Publication 100*. The one exception was that of the small intestine wall. In *Publication 100*, a single tubular structure was adopted, while in the present report, a hexagonal array of tubular structures was adopted to allow for wall segment cross-fire. All radiation transport simulations were performed using MCNPX version 2.6 (Pelowitz, 2008). Maximum particle energies considered were 10 MeV for electrons and 12 MeV for alpha particles.

REFERENCES

Bahadori, A.A., Johnson, P.B., Jokisch, D.W., Eckerman, K.F., Bolch, W.E., 2011. Response functions for computing absorbed dose to skeletal tissues from neutron irradiation. Phys. Med. Biol. 56, 6873–6897.

Beddoe, A.H., Darley, P.J., Spiers, F.W., 1976. Measurements of trabecular bone structure in man. Phys. Med. Biol. 21, 589–607.

Beddoe, A.H., Spiers, F.W., 1979. A comparative study of the dosimetry of bone-seeking radionuclides in man, rhesus monkey, beagle, and miniature pig. Radiat. Res. 80, 423–439.

Berger, M.J., 1963. Monte Carlo calculation of the penetration and diffusion of fast charged particles. In: Alder, B., Fernbach, S., Rotenberg, M. (Eds.), Methods in Computational Physics. Academic Press, New York, pp. 135–215.

Berger, M.J., Hubbell, J.H., 1987. XCOM: photon cross sections on a personal computer. NBSIR 87-3597. National Bureau of Standards (former name of NIST), Gaithersburg, MD.

Bolch, W.E., Eckerman, K.F., Sgouros, G., Thomas, S.R., 2009. MIRD Pamphlet No. 21: A generalized schema for radiopharmaceutical dosimetry - Standardization of Nomenclature. J. Nucl. Med. 50, 477–484.

Bouchet, L.G., Jokisch, D.W., Bolch, W.E., 1999. A three-dimensional transport model for determining absorbed fractions of energy for electrons within trabecular bone. J. Nucl. Med. 40, 1947–1966.

Brown, L., Feynman, R., 1952. Radiative corrections to Compton scattering. Phys. Rev. 85, 231–244.

Chadwick, M.B., Young, P.G., Chiba, S., et al., 1999. Cross section evaluations to 150 MeV for accelerator-driven systems and implementation in MCNPX. Nucl. Sci. Eng. 131, 293–328.

Cristy, M., 1980. Mathematical phantoms representing children of various ages for use in estimates of internal dose. Oak Ridge National Laboratory Report ORNL/NUREG/TM-367.

Cristy, M., Eckerman, K.F., 1987. Specific absorbed fractions of energy at various ages for internal photon sources. Oak Ridge National Laboratory Report ORNL/NUREG/TM-8381, Vol. 1-7.

Darley PJ 1972 Measurement of linear path length distributions in bone and bone marrow using a scanning technique Leeds, UK, University of Leeds.

Eckerman, K.F., Westfal, R.J., Ryman, J.C., Cristy, M., 1994. Availability of nuclear decay data in electronic form, including beta spectra not previously published. Health Phys. 67, 338–345.

Eckerman, K.F. Stabin, M.G., 2000. Electron absorbed fractions and dose conversion factors for marrow and bone by skeletal regions. Health Phys. 78, 199–214.

Halbleib, J.A., Kensek, R.P., Valdez, G.D., et al., 1992. TS Version 3.0: the Integrated TIGER Series of Coupled Electron/Photon Monte Carlo Transport Codes SAND91-1634. Sandia National Laboratories, Albuquerque, New Mexico 87185 and Livermore, California 94550, US.

Hough, M., Johnson, P., Rajon, D., Jokisch, D., Lee, C., Bolch, W.E., 2011. An image-baed skeletal dosimetry model for the ICRP reference adult male -

internal electron sources. Phys. Med. Biol. 56, 2309–2346.

IAEA, 1996. Basic Safety Standards for Direct Methods for Measuring Radionuclides in the Human Body. Safety Series 114. International Atomic Energy Agency, Vienna, Austria.

ICRU, 1992. Photon, electron, proton, and neutron interaction data for body tissues *ICRU Report 46 (Bethesda, MD: International Commission on Radiation Units and Measurements).*

ICRU, 1993. Stopping powers and ranges for protons and alpha particles *ICRU Report 49 (Bethesda, MD: International Commission on Radiation Units and Measurements).*

ICRP, 1975. Report on the Task Group on Reference Man. ICRP Publication 23. Pergamon Press, Oxford, UK.

ICRP, 1977. Recommendations of the International Commission on Radiological Protection. ICRP Publication 26. Ann. ICRP 1(3).

ICRP, 1979. Limits for intake of radionuclides by workers. ICRP Publication 30, Part 1. Ann. ICRP 2(3/4).

ICRP, 1980. Limits for intakes of radionuclides by workers. ICRP Publication 30, Part 2. Ann. ICRP 4(3/4).

ICRP, 1981. Limits for intakes of radionuclides by workers. ICRP Publication 30, Part 3. Ann. ICRP 6 (2/3).

ICRP, 1983. Radionuclide transformations: energy and intensity of emissions. ICRP Publication 38. Ann. ICRP 11-13.

ICRP, 1986. The metabolism of plutonium and related elements. ICRP Publication 48, Ann. ICRP 16(2/3).

ICRP, 1988a. Individual monitoring for intakes of radionuclides by workers: design and interpretation. ICRP Publication 54, Ann. ICRP 19(1-3).

ICRP, 1988b. Limits for intakes of radionuclides by workers: An Addendum. ICRP Publication 30, Part 4. Ann. ICRP 19(4).

ICRP, 1989. Age-dependent doses to members of the public from intake of radionuclides. ICRP Publication 56, Part 1. Ann. ICRP 20(2).

ICRP, 1991. 1990 Recommendations of the ICRP. ICRP Publication 60. Ann. ICRP 21(1-3).

ICRP, 1993a. Protection against radon-222 at home and work. ICRP Publication 65. Ann. ICRP 23(2).

ICRP, 1993b. Age-dependent doses to members of the public from intake of radionuclides: Part 2, Ingestion dose coefficients. ICRP Publication 67. Ann. ICRP 23(3/4).

ICRP, 1994a. Human respiratory tract model for radiological protection. ICRP Publication 66. Ann. ICRP 24(1-3).

ICRP, 1994b. Dose coefficients for intake of radionuclides by workers. ICRP Publication 68. Ann. ICRP 24(4).

ICRP, 1995a. Basic anatomical and physiological data for use in radiological protection: The skeleton. ICRP Publication 70. Ann ICRP 25(2).

ICRP, 1995b. Age-dependent doses to members of the public from intake of radionuclides: Part 3, Ingestion dose coefficients. ICRP Publication 69. Ann. ICRP 25(1).

ICRP, 1995c. Age-dependent doses to members of the public from intake of radionuclides: Part 4, Inhalation dose coefficients. ICRP Publication 71. Ann. ICRP 25(3/4).

ICRP, 1996. Age-dependent doses to members of the public from intake of radionuclides: Part 5 Compilation of ingestion and inhalation dose coefficients. ICRP Publication 72. Ann. ICRP 26(1).

ICRP, 1997a. General principles for the radiation protection of workers. ICRP Publication 75, Ann. ICRP 27(1).

ICRP, 1997b. Individual monitoring for internal exposure of workers – Replacement of ICRP Publication 54. ICRP Publication 78. Ann. ICRP 27(3/4).

ICRP, 2001. Dose to the embryo and fetus from intakes of radionuclides by the mother. ICRP Publication 88. Ann. ICRP 31(1-3).

ICRP, 2002a. Basic anatomical and physiological data for use in radiological protection: reference values. ICRP Publication 89. Ann. ICRP 32(3-4).

ICRP, 2002b. Guide for the practical applications of the ICRP Human Respiratory Tract Model. Supporting Guidance 3. Ann. ICRP 32(1/2).

ICRP, 2004. Doses to the infant from radionuclides ingested in mothers' milk. ICRP Publication 95, Ann. ICRP 34(3/4).

ICRP, 2005. Basis for dosimetric quantities used in radiological protection. Committee 2 Consultation Draft. www.icrp.org (May 2004).

ICRP, 2006. Human alimentary tract model for radiological protection. ICRP Publication 100. Ann. ICRP 36(1/2).

ICRP, 2007. The 2007 Recommendations of the International Commission on Radiological Protection. ICRP Publication 103. Ann. ICRP 37(2-4).

ICRP, 2008. Nuclear decay data for dosimetric calculations. ICRP Publication 107. Ann. ICRP 38(3).

ICRP, 2009. Adult reference computational phantoms. ICRP Publication 110. Ann. ICRP 39(2).

ICRP, 2010. Conversion coefficients for radiological protection quantities for external radiation exposures. ICRP Publication 116. Ann. ICRP 40(1).

ICRP, 2015. Occupational Intakes of Radionuclides: Part 1. ICRP Publication 130. Ann. ICRP 44(2).

Johnson, P.B., Bahadori, A.A., Eckerman, K.F., Lee, C., Bolch, W.E., 2011. Response functions for computing absorbed dose to skeletal tissues from photon irradiation – an update. Phys. Med. Biol. 56, 2347–2366.

Jokisch, D.W., Rajon, D.A., Bahadori, A.A., Bolch, W.E., 2011a. An image-based skeletal dosimetry model for the ICRP reference adult male – specific absorbed fractions for neutron-generated recoil protons. Phys. Med. Biol. 56, 6857–6872.

Jokisch, D.W., Rajon, D.A., Patton, P.W., Bolch, W.E., 2011b. Methods for the inclusion of shallow marrow and adipose tissue in pathlength-based skeletal dosimetry. Phys. Med. Biol. 56, 2699–2713.

Kawrakow, I., 2002. Electron impact ionization cross sections for EGSnrc. Med. Phys. 29, 1230.

Kawrakow, I., Mainegra-Hing, E., Rogers, D.W.O., et al., 2009. The EGSnrc Code System: Monte Carlo Simulation of Electron and Photon Transport. PIRS Report 701. National Research Council of Canada, Ottawa.

Kirk, B.L., 2010. Overview of Monte Carlo radiation transport codes. Radiat. Meas. 45, 1318–1322.

Lee, C., Lamart, S., Moroz, B.E., 2013. Computational lymphatic node models in pediatric and adult hybrid phantoms for radiation dosimetry. Phys. Med. Biol. 58, N59–N82.

Nelson, W.R., Hirayama, H., Rogers, D.W.O., 1985. The EGS4 Code System. SLAC Report 265. Stanford Linear Accelerator Center, Stanford, CA.

Niita, K., Matsuda, N., Iwamoto, Y., et al., 2010. PHITS - Particle and Heavy Ion Transport code System, Version 2.23. Japan Atomic Energy Agency, Tokai-mura, Japan.

Øverbø, I., Mork, K.J., Olsen, A., 1973. Pair production by photons: exact calculations for unscreened atomic fields. Phys. Rev. A8, 668–684.

Pelowitz, D.B., 2008. MCNPX User's Manual, Version 2.6.0. LA-CP-07-1473, Los Alamos National Laboratory Los Alamos, NM, USA.

Petoussi-Henss N, WE Bolch, M Zankl, G Sgouros and B Wessels 2007 Patient-specific scaling of reference S-values for cross-organ radionuclide S-values: What is appropriate? *Radiat Prot Dosimetry* 127, 192-196.

Rajon, D.A., Bolch, W.E., 2003. Marching cube algorithm: Review and trilinear interpolation adaptation for image-based dosimetric models. Comput. Med. Image Graph. 27, 411–435.

Rajon, D.A., Jokisch, D.W., Patton, P.W., Shah, A.P., Watchman, C.J., Bolch, W.E., 2002. Voxel effects within digital images of trabecular bone and their consequences on chord-length distribution measurements. *Phys. Med. Biol.* 47, 1741–1759.

Reverter, J., Feliu, E., Climent, C., Rozman, M., Berga, L., Rozman, C., 1993. Sterological study of human bone marrow adipocytes: a comparison of four methods for estimating size distributions. Pathol. Res. Pract. 189, 1215–1220.

Seltzer, S.M., Berger, M.J., 1985. Bremsstrahlung spectra from electron interactions with screened atomic nuclei and orbital electrons. Nucl. Instrum. Methods Phys. Res. Sect. B12, 95–134.

Seltzer, S.M., Berger, M.J., 1986. Bremsstrahlung energy spectra from electrons with kinetic energy from 1 keV to 10 GeV incident on screened nuclei and orbital electrons of neutral atoms with Z = 1-100. Atom. Data Nucl. Data Tables 35, 345–418.

Seuntjens, J.P., Kawrakow, I., Borg, J., et al., 2002. Calculated and measured air-kerma response of ionization chambers in low and medium energy photon beams. In: Seuntjens, J.P., Mobit, P. (Eds.), Recent Developments in Accurate Radiation Dosimetry,Proceedings of an International Workshop, Montreal, July 14–18, 2002. Symposium Proceedings 13, Medical Physics Publishing, Madison, USA. pp. 69–84.

Shah, A.P., Bolch, W.E., Rajon, D.A., Patton, P.W., Jokisch, D.W., 2005. A paired-image radiation transport (PIRT) model for skeletal dosimetry. J. Nucl. Med. 46, 344–353.

Snyder WS, MR Ford, GG Warner and EE Watson 1975 ‘S’ absorbed dose per unit cumulated activity for selected radionuclides and organs. MIRD Pamphlet No. 11, Revised. (New York, NY: Society of Nuclear Medicine)

Snyder WS 1970 Estimation of absorbed fraction of energy from photon sources in

body organs. In: Medical Radionuclides: Radiation dose and effects. Editors: RJ Cloutier, CL Edwards, WS Snyder. (US Atomic Energy Commission, Division of Technical Information (CONF-691212) pp. 33-49.

Snyder WS, MR Ford and GG Warner 1978 Estimates of specific absorbed fractions for photon sources uniformly distributed in various organs of a heterogeneous phantom. MIRD Pamphlet No. 5, Revised. (New York, NY: Society of Nuclear Medicine)

Spiers, F.W., 1968. Dosimetry at interfaces with special reference to base *Proc. Symp. on Microdosimetry (EAEC Publication)* pp 473–508.

Spiers, F.W., Beddoe, A.H., 1977. 'Radial' scanning of trabecular bone: Consideration of the probability distributions of path lengths through cavities and trabeculae. Phys. Med. Biol. 22, 670–680.

Spiers, F.W., Beddoe, A.H., Whitwell, J.R., 1978a. Mean skeletal dose factors for beta-particle emitters in human bone. Part i: Volume-seeking radionuclides. Br. J. Radiol. 51, 622–627.

Spiers, F.W., Beddoe, A.H., Whitwell, J.R., 1981. Mean skeletal dose factors for beta-particle emitters in human bone. Part ii: Surface-seeking radionuclides. Br. J. Radiol. 54, 500–504.

Spiers, F.W., Whitwell, J.R., Beddoe, A.H., 1978b. Calculated dose factors for the radiosensitive tissues in bone irradiated by surface-deposited radionuclides. Phys. Med. Biol. 23, 481–494.

Tsoulfanidis, N., 1983. *Measurement and detection of radiation* Hemisphere Publishing Corp.

Waters, L.S., 2002. MCNPX User's Manual, Version 2.3.0. Report LA-UR-02-2607. Los Alamos National Laboratory, Los Alamos, NM.

Whitwell, J.R., 1973. Theoretical investigations of energy loss by ionizing particles in bone Leeds, UK, University of Leeds.

Whitwell, J.R., Spiers, F.W., 1976. Calculated beta-ray dose factors for trabecular bone. Phys. Med. Biol. 21, 16–38.

Young, P.G., Arthur, E.D., Chadwick, M.B., 1996. Comprehensive nuclear model calculations: theory and use of the GNASH code. In: Reffo, G.A. (Ed.), IAEA Workshop on Nuclear Reaction Data and Nuclear Reactors—Physics Design, and Safety, Trieste, 15 April–17 May, pp. 227–404.

Zankl, M., Eckerman, K., Bolch, W.E., 2007. Voxel-based models representing the male and female ICRP reference adult – the skeleton. Radiat. Prot. Dosim. 127, 174–186.

Zankl, M., Fill, U., Petoussi-Henss, N., Regulla, D. 2002. Organ dose conversion coefficients for external photon irradiation of male and female voxel models. Phys. Med. Biol. 47, 2367–2385.

Zankl, M., Petoussi-Henss, N., Fill, U., Regulla, D., 2003. The application of voxel phantoms to the internal dosimetry of radionuclides. Radiat. Prot. Dosim. 105, 539–548.

Zankl, M., Schlattl, H., Petoussi-Henss, N., Hoeschen, C., 2012. Electron specific absorbed fractions for the adult male and female ICRP/ICRU reference computational phantoms. Phys. Med. Biol. 57, 4501–4526.

1405 Ziegler, J.F., Biersack, J.P., Ziegler, M., et al., 2003. SRIM – the Stopping and Range
1406 of Ions in Matter. American Nuclear Society, La Grange Park, USA.
1407 Available at: www.srim.org (last accessed December 2011).
1408

1409

ANNEX A

Table A.1. Masses of Target Tissues in the Reference Adult Male and Female.

Target Tissue	Mass (kg)		Acronym	Reference
	Male	Female		
Brain	1.52	1.35	Brain	See note 1
Pituitary gland	7.12×10^{-4}	6.82×10^{-4}	P-gland	See note 1
Eye	1.57×10^{-2}	1.54×10^{-2}	Eye-lens	See note 2
Oral mucosa	0.0358	0.0225	O-mucosa	See note 2
Tongue	0.0745	0.0610	Tongue	See note 1
Tonsils	0.00350	0.00341	Tonsils	See note 1
Salivary glands	0.0853	0.0703	S-gland	See note 1
Oesophagus	9.5×10^{-5}	8.8×10^{-5}	Oesophagus	See note 3
Thymus	0.0293	0.0229	Thymus	See note 1
Breast	0.0254	0.500	Breast	See note 1
ET1 basal cells	2.0×10^{-5}	1.7×10^{-5}	ET1-bas	See note 4
ET2 basal cells	4.5×10^{-4}	3.9×10^{-4}	ET2-bas	See note 4
Extrathoracic lymph nodes	0.015	0.012	LN-ET	See note 4
Bronchi basal cells	4.3×10^{-4}	3.9×10^{-4}	Bronch-bas	See note 4
Bronchi secretary cells	8.6×10^{-4}	7.8×10^{-4}	Bronch-sec	See note 4
Bronchiolar secretary cells	1.9×10^{-3}	1.9×10^{-3}	Bchiol-sec	See note 4
Alveolar-interstitial	1.10	0.90	AI	See note 4
Thoracic lymph nodes	0.015	0.012	LN-Th	See note 4
Stomach	6.16×10^{-4}	6.16×10^{-4}	St-stem	See note 3
Small intestine	0.00371	0.00345	SI-stem	See note 3
Right colon	0.00135	0.00119	RC-stem	See note 3
Left colon	0.00126	0.0016	LC-stem	See note 3
Sigmoid colon	7.59×10^{-4}	6.99×10^{-4}	RS-stem	See note 3
Red (active) marrow	1.17	0.90	R-marrow	See note 1
Endosteal cells	0.544	0.407	Endost-BS	See note 5
Adrenals	0.0174	0.0155	Adrenals	See note 1
Thyroid	0.0234	0.0195	Thyroid	See note 1
Heart	0.339	0.256	Ht-wall	See note 1
Liver	2.36	1.81	Liver	See note 1
Gall bladder	0.0124	0.00948	GB-wall	See note 1
Kidneys	0.422	0.357	Kidneys	See note 1
Pancreas	0.174	0.145	Pancreas	See note 1
Spleen	0.228	0.187	Spleen	See note 1
Systemic lymph	0.148	0.118	LN-Sys	See note 6
Ureters	0.0187	0.0172	Ureters	See note 1
Uterus	-	0.0915	Uterus	See note 1
Prostate	0.0199	-	Prostate	See note 1
Urinary bladder	0.0511	0.0408	UB-wall	See note 1
Ovaries	-	0.0118	Ovaries	See note 1
Testes	0.0372	-	Testes	See note 1
Muscle	29.8	17.9	Muscle	See note 1
Adipose tissue	18.5	22.8	Adipose	See note 7
Skin	3.30	2.30	Skin	See note 1

Notes:

1. Based on Table 2.8 of *Publication 89* plus the blood content per *Publication 89*, p. 142.
2. Based on Table A.1 of *Publication 110* plus 0.010% of total blood mass.
3. Based on geometric model of *Publication 100* assuming a tissue density of 1.03 g/cm^3.
4. Based on Table 5.3 of *Publication 89*.
5. Based on Table 3.2 of *Publication 116*.
6. Adopted mass of all lymph nodes as 178 and 143 g in male and female, respectively.

7. Sum of residual tissue masses in Table A.1 of *Publication 110* plus blood per *Publication 89*, p. 142.

1412

Table A.2. Masses of Source Regions in the Reference Adult Male and Female.

Source Region	Mass (kg)		Acronym	Reference
	Male	Female		
Brain	1.45	1.30	Brain	*Publication 89*, Table 2.8
Pituitary gland	6×10^{-4}	6.0×10^{-4}	P-gland	*Publication 89*, Table 2.8
Eyes	0.015	0.015	Eyes	*Publication 89*, Table 2.8
Oral cavity	-	-	O-cavity	
Oral mucosa	0.0358	0.0225	O-mucosa	*Publication 110*, Table A.1
Salivary glands	0.085	0.070	S-glands	*Publication 89*, Table 2.8
Teeth surface	-	-	Teeth-S	
Teeth volume	0.050	0.040	Teeth-V	*Publication 89*, Table 2.8
Tongue	0.073	0.060	Tongue	*Publication 89*, Table 2.8
Tonsils	0.003	0.003	Tonsils	*Publication 89*, Table 2.8
Oesophagus - content	-	-	Oesophag-c	
Oesophagus	0.040	0.035	Oesophagus	*Publication 89*, Table 2.8
Breast	0.025	0.50	Breast	*Publication 89*, Table 2.8
Stomach contents	0.25	0.23	St-cont	*Publication 89*, Table 2.8
Stomach wall	0.15	0.14	St-wall	*Publication 89*, Table 2.8
Small intestine contents	0.35	0.28	SI-cont	*Publication 89*, Table 2.8
Small intestine villi			SI-villi	
Small intestine wall	0.65	0.60	SI-wall	*Publication 89*, Table 2.8
Right colon content	0.15	0.16	RC-cont	*Publication 89*, Table 2.8
Right colon wall	0.15	0.145	RC-wall	*Publication 89*, Table 2.8
Left colon content	0.075	0.080	LC-cont	*Publication 89*, Table 2.8
Left colon wall	0.15	0.145	LC-wall	*Publication 89*, Table 2.8
Sigmoid colon content	0.075	0.080	RS-cont	*Publication 89*, Table 2.8
Sigmoid colon wall	0.070	0.070	RS-wall	*Publication 89*, Table 2.8
ET1 surface	-	-	ET1-sur	
ET2 surface	-	-	ET2-sur	
ET2 bound region	2.47×10^{-3}	2.14×10^{-3}	ET2-bnd	See note 2
ET2 sequestered region	4.50×10^{-4}	3.89×10^{-4}	ET2-seq	See note 2
Extrathoracic lymph nodes	0.015	0.012	LN-ET	*Publication 66*, Table 5
Bronchial surface	-	-	Bronchi	
Bronchial bound region	1.73×10^{-3}	1.55×10^{-3}	Bronchi-b	See note 2
Bronchial sequestered region	2.92×10^{-4}	2.62×10^{-4}	Bronchi-q	See note 2
Bronchiolar surface	-	-	Bronchiole	
Bronchiolar bound region	4.89×10^{-3}	4.70×10^{-3}	Brchiole-b	See note 2
Bronchiolar sequestered region	1.25×10^{-3}	1.20×10^{-3}	Brchiole-q	See note 2
Alveolar-interstitial	1.10	0.90	AI	See note 2
Thoracic lymph nodes	0.015	0.012	LN-Th	*Publication 66*, Table 5
Cortical bone surface	-	-	C-bone-S	
Cortical bone	4.40	3.20	C-bone-V	*Publication 89*, Table 2.8
Trabecular bone surface	-	-	T-bone-S	
Trabecular bone	1.10	0.80	T-bone-V	*Publication 89*, Table 2.8
Cortical bone marrow	0.279	0.257	C-marrow	
Trabecular bone marrow	3.37	2.44	T-marrow	
Red (active) marrow	1.17	0.90	R-marrow	*Publication 89*, Table 2.8
Yellow (inactive) marrow	2.48	1.80	Y-marrow	*Publication 89*, Table 2.8
Blood	5.60	4.10	Blood	*Publication 89*, Table 2.8
Thyroid	0.020	0.017	Thyroid	*Publication 89*, Table 2.8
Thymus	0.025	0.020	Thymus	*Publication 89*, Table 2.8

Heart content	0.51	0.37	Ht-cont	*Publication 89*, Table 2.8
Heart	0.33	0.25	Ht-wall	*Publication 89*, Table 2.8
Adrenals	0.014	0.013	Adrenals	*Publication 89*, Table 2.8
Gall bladder content	0.058	0.048	GB-cont	*Publication 89*, Table 2.8
Gall bladder	0.010	0.008	GB-wall	*Publication 89*, Table 2.8
Kidneys	0.310	0.275	Kidneys	*Publication 89*, Table 2.8
Liver	1.80	1.40	Liver	*Publication 89*, Table 2.8
Systemic lymph	0.148	0.118	LN-Sys	See note 2
Pancreas	0.14	0.12	Pancreas	*Publication 89*, Table 2.8
Spleen	0.15	0.13	Spleen	*Publication 89*, Table 2.8
Testes	0.035	-	Testes	*Publication 89*, Table 2.8
Ovaries	-	0.011	Ovaries	*Publication 89*, Table 2.8
Ureters	0.016	0.015	Ureters	*Publication 89*, Table 2.8
Urinary bladder	0.050	0.040	UB-wall	*Publication 89*, Table 2.8
Urinary bladder content	0.20	0.20	UB-cont	
Uterus	-	0.080	Uterus	*Publication 89*, Table 2.8
Prostate	0.017	-	Prostate	*Publication 89*, Table 2.8
Muscle	29.0	17.5	Muscle	*Publication 89*, Table 2.8
Adipose	20.47	23.90	Adipose	See note 3
Cartilage	1.10	0.90	Cartilage	*Publication 89*, Table 2.8
Skin	3.30	2.30	Skin	*Publication 89*, Table 2.8

Notes:

1. Based on geometric model of *Publication 100* assuming a tissue density of 1.03 g/cm^3.
2. Derived from information in *Publications 66* and *89*. Mass of all lymph nodes is 178 and 143 g in male and female, respectively.
3. Sum of residual tissue masses in *Publication 110*, Table A.1.

1413

ANNEX B

DESCRIPTION OF ELECTRONIC FILES

The alpha, electron, photon, and neutron SAF files listed below have the same file structure. The files are formatted as direct access files and are accompanied by two index files which enable one to compute the SAF record of interest in the SAF files given the acronyms of the target organ and source region. This brief note illustrates how to use the files and how to derive the SAFs for Other Tissue as a source region.

B.1. Alpha, Electron and Photon SAF Files

The SAF files are:

RCP-AF_Alpha_2015-08-04.SAF RCP-AF_Electron_2015-08-04.SAF
RCP-AF_Photon_2015-08-04.SAF RCP-AM_Alpha_2015-08-04.SAF
RCP-AM_Electron_2015-08-04.SAF
RCP-AM_Photon_2015-08-04.SAF

where AF and AM denote adult female and adult male, respectively.

Each file has 5 header records thus the 6th record is the first SAF record and the last record is 3859 (47 target tissues x 82 source regions + 5 header records). The record length varies with radiation type. The record length of the electron and photon files is 315 and record length in the alpha SAF files is 270. The accompanying carriage return and line feed (CrLf) are not included in these lengths. The fields of the data record are

Target Tissue	10 characters	Acronym of target; e.g. UB-wall
Dummy	2 characters	Actually the characters "<-"
Source Region	10 characters	Source region acronym; e.g. UB-cont
SAF(1 to n)	E10.0	n SAF values (kg^{-1})
Ecut†	E10.0	Lowest energy of non-zero SAF
Icut	I3	Energy Index of Ecut
CrLf	2 characters	Carriage return and line feed

†Ecut format in alpha SAF files is F5.0

The number of energies n addressed in the electron and photon files is 28. The alpha file addresses 24 energies and as noted above, in the alpha SAF file the Ecut parameter is of length 5 (F5.0).

The 4th record of each file lists the energies of the radiation corresponding to the SAF values. This record can be read assuming the above structure with the SAF fields containing the energy of the radiation corresponding to the SAF values. That is, for the 4th record in the electron and photon SAF files, the value of E(i) = SAF (i), i = 1

to 28. The unit of the energy values is MeV.

The Icut field contains the index of the lowest energy value for a non-zero SAF(T<-S). If all SAFs are zero then Icut is set to 0. If Icut has a value of *j* then nonzero SAF values are reported for energy values ranging from E(*j*) to E(n) where n is 28 in the electron/photon SAF files and 24 in the alpha SAF files. That is the number of non-zero SAF values is n – j + 1.

Some compilers require that the statement opening a file for random access specify the record length include the CrLf (add two to the above noted values) and others do not include the CrLf.

B.2. Neutron SAF Files

The neutron SAF files are:

RCP-AF_Neutron_2015-08-04.SAF
RCP-AM_Neutron_2015-08-04.SAF

where AF and AM denote adult female and adult male, respectively.
The neutron SAF file tabulates the SAF of the emitted neutron energy for each of the 47 target tissues and 82 source regions for those radionuclides in *Publication 107* for which spontaneous fission is a decay mode. The 28 radionuclides are: U-238, Pu-236, Pu-238, Pu-240, Pu-242, Pu-244, Cm-240, Cm-242, Cm-244, Cm-245, Cm-246, Cm-248, Cm-250, Cf-246, Cf-248, Cf-249, Cf-250, Cf-252, Cf-254, Es-253, Es-254, Es-254m, Es-255, Fm-252, Fm-254, Fm-255, Fm-256, and Fm-257.

The fourth record in these files tabulates the spectral-average w_R for each radionuclide. The data format of the neutron files is

Target Tissue	10 characters	Acronym of target; e.g. UB-wall
Dummy	2 characters	Actually the characters "<-"
Source Region	10 characters	Source region acronym; e.g. UB-cont
SAF(1 to 28)	E10.0	28 SAF values (kg^{-1})
CrLf	2 characters	Carriage return and line feed

The record length in these files is 302. Some compilers require that the statement opening a file for random access specify the record length include the CrLf (add two to the above noted values) and others do not include the CrLf.

B.3. Target and Source Index Files

The files TOrgans.NDX and SRegions.NDX list the target tissues and source regions, respectively, in their order of appearance within the SAF files. The SAF files address 47 target tissues being irradiated by 82 source regions. The record number *irec* of the *SAF* for irradiation of the i^{th} target region by the j^{th} source region is

$$irec = 47\ (j - 1) + i + 5$$

where 70 is the number of target tissues addressed in the files. For example, the record addressing the irradiation of the 21th target region *Brain* by 10th source region *St-cont* is

$$irec = 47\ (10 - \ 1) + \ 21 + 5 = \ 449$$

which can be confirmed by opening an SAF file in an editor which indexes the file records.

B.4. Deriving SAFs for Other Tissues

Frequently systemic biokinetic models will indicate deposition from *Blood* into a compartment (or compartments) labeled as *Other* (or *Other*_1, *Other*_2, etc). To address this source region, one must derive the *SAF* for the target tissues r_T being irradiated by this source region; i.e. calculate SAF(r_T<-*Other*). This may be calculated as

$$SAF(r_T \leftarrow Other) = \frac{1}{M_{Other}} \sum_{r_S} M_{r_S}\, SAF(r_T \leftarrow r_S) \qquad \text{(B.1)}$$

where the summation extends over source regions not explicit noted in the systemic biokinetic model. Source regions which are potential candidates are noted in SRegions.NDX and marked with a gender-specific attribute *ID*. An *ID* value of 1 includes the source is a candidate for inclusion in Other (provided it is not present in the biokinetic model). The *ID* column follows after the gender-specific mass of the tissues. The mass of *Other* is the sum of the masses of the source regions comprising *Other*. Eqn 1 is the so-called additive approach. Note that neither *C-bone-S* nor *T-bone-S* (source regions representing activity on mineral bone surfaces) are part of *Other* as no volume is associated with these regions.

B.5. Limiting SAF Values

The electron, photon, and alpha SAF files include limiting SAF values as the energy of the radiation approaches zero; i.e. $\lim_{E\to 0} SAF(r_T \leftarrow r_S; E)$. The limiting value at E = 0 and the nonzero values at 10 keV and above are used to derive values, by interpolation, at 1 and 5 keV in the electron and photon files and at 1 and 1.5 MeV in the alpha files. The additional low energy values are helpful in SAF interpolations and extrapolations. The limiting SAF values are derived as:

Solid organs:

$$\lim_{E\to 0} SAF(r_T \leftarrow r_S) = \begin{cases} \dfrac{1}{M_{r_T}}, & \text{if } r_S = r_T \\ 0, & \text{if } r_S \neq r_T \end{cases} \quad \text{(B.2)}$$

HRTM: Limiting SAFs for a source in the bound region of the airways

$$\lim_{E\to 0} SAF(ET2\ bas \leftarrow ET2\ bnd) = \frac{0.182}{M_{ET2\ bas}} \quad \text{(B.3a)}$$

$$\lim_{E\to 0} SAF(Bronch\ bas \leftarrow Bronchi\ b) = \frac{0.250}{M_{Bronch\ bas}} \quad \text{(B.3b)}$$

$$\lim_{E\to 0} SAF(Bronch\ sec \leftarrow Bronchi\ b) = \frac{0.500}{M_{Bronch\ sec}} \quad \text{(B.3c)}$$

$$\lim_{E\to 0} SAF(Bchiol\ sec \leftarrow Brchiole\ b) = \frac{0.400}{M_{Bchiol\ sec}} \quad \text{(B.3d)}$$

The numerical values in Eqns B.3 are the absorbed fractions at the lowest energy; e.g. 10 keV in the case of photon and electrons, and 2 MeV for alpha particles. The limiting values for the sequestered source regions are zero.

Segments of the HATM: Limiting SAF for a source in the wall is

$$\lim_{E\to 0} SAF(X_{wall} \leftarrow Y_{wall}) = \begin{cases} \dfrac{1}{M_{Y_{wall}}}, & \text{if } X = Y \\ 0, & \text{if } X \neq Y \end{cases} \quad \text{(B.4)}$$

and for the source in the mucosa layer of the wall

$$\lim_{E\to 0} SAF(X_{wall} \leftarrow Y_{mucosa}) = \begin{cases} \dfrac{1}{M_{Y_{mucosa}}}, & \text{if } X = Y \\ 0, & \text{if } X \neq Y \end{cases} \quad \text{(B.5)}$$

Blood:

$$\lim_{E\to 0} SAF(r_T \leftarrow Blood) = \frac{f_{r_T}}{M_{r_T}} \quad \text{(B.6)}$$

where f_{r_T} is the mass fraction of the body's blood in the target r_T per *Publications 89* and *110*.